Building and Environment 275 (2025) 112765

Contents lists available at ScienceDirect

Building and Environment

journal homepage: www.elsevier.com/locate/buildenv

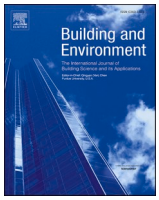

Hotels as quarantine facilities with airborne virus controls

Hamed Sobhani, Shengwei Zhu, Jelena Srebric *

Department of Mechanical Engineering, University of Maryland, College Park, MD, USA

ARTICLE INFO

Keywords:
Multi-zone modeling
Viral aerosol transmission
Quarantine hotel
Ventilation
COVID-19
Air cleaning strategies and devices

ABSTRACT

During the COVID-19 pandemic, hotels were converted into quarantine facilities, often lacking adequate air-cleaning infrastructure. This study aimed to design effective air-cleaning strategies for controlling viral aerosol transmission, especially inter-zonal transmission, which can undermine the quarantine effectiveness in isolating infected individuals. We developed a validated multi-zone model for an actual quarantine hotel to evaluate performance of air-cleaning strategies. Importantly, we developed the inter-zonal air exchange rate (zACH) index to evaluate the air-cleaning infrastructure effectiveness in reducing inter-zonal transmission of aerosols. The zACH improved significantly from a total of 0.4 1/h of clean air in the baseline strategy without additional air-cleaning to a total of 3.5, 2.8, and 1.7 1/h of clean air for strategies with only GUV fixtures, only HEPA air cleaners, and only air curtains, respectively. We also evaluated the combined air-cleaning strategies that integrated these systems, including air hygiene strategies with fewer devices complementing each other. Our best air hygiene strategy, resulting in the zACH of 8.5 1/h, reduced maximum individual infectious exposure risk below 0.4 % in rooms and below 1.6 % in corridors for a generation rate of 50 quanta/h. Importantly, air-cleaning effectiveness was not linearly proportional to the number of deployed devices, highlighting the importance of balancing performance with installation costs and energy consumption considerations. These findings offer an analytical framework for enhancing infection control in quarantine hotels and provide insights for public health mitigation strategies during pandemics.

1. Introduction

Since late December 2019, we have experienced the Coronavirus Disease 2019 (COVID-19), a major pandemic of the century. At the onset, with no vaccine or treatment available for this newly emerged deadly virus, isolating exposed individuals or those with mild symptoms for 14 days [1] was considered an effective measure to minimize SARS-CoV-2 transmission. This quarantine strategy continued throughout the pandemic due to the virus's extremely high transmission rate (up to 0.18, equivalent to an effective reproduction number of 2.52) [2]. This high transmission rate was partly due to aerosol transmission, which was recognized as a significant route for the spread of COVID-19 by both the World Health Organization (WHO) [3] and the US Center for Disease Control (CDC) [4].

Hotels have been effectively utilized as quarantine facilities to isolate travelers or local residents who were exposed to or infected with COVID-19 and had no other place for isolation [5]. Compared to other buildings, hotels are particularly well-suited for quarantine purposes [5]. With many guest rooms, hotels can assign each guest to an isolated room with an attached bathroom and amenities, ensuring zero contact. For quarantine hotel design, the exhaust fan installed in the attached bathroom is expected to create negative pressure, minimizing viral aerosols from leaking into the corridors [6]. Although hotels designated for quarantine were adapted based on the guidelines and standard operating procedures by local public health authorities [5,7], quarantine systems could still fail to minimize SARS-CoV-2 transmission. For instance, Grout et al. identified 32 quarantine system failures in Australia and New Zealand by June 15, 2021 [8], with 6.1 failures per 1000 COVID-19-positive travelers passing through quarantine hotels. One such failure resulted in a COVID-19 outbreak with more than 800 deaths, highlighting the need for improvements or alternative approaches to hotel-based quarantine. Meanwhile, interviews with quarantine guests revealed major concerns about community risks identified in quarantine [9], hotel hygiene, and disinfection [5]. Operable windows and sufficient ventilation were considered crucial for well-being in quarantine hotels [10]. In addition, a transmission event suggested that cross-ventilation via the aerosol route might account for confirmed COVID-19 cases in adjacent hotel rooms [6]. A previous study on influenza transmission in a

* Corresponding author at: 3143 Glenn L. Martin Hall, College Park, MD 20740, USA.
E-mail address: jsrebric@umd.edu (J. Srebric).

https://doi.org/10.1016/j.buildenv.2025.112765
Received 29 August 2024; Received in revised form 23 January 2025; Accepted 20 February 2025
Available online 28 February 2025

low-ventilation dormitory with a similar floor plan to the hotel, also confirmed the potential for aerosol transmission between two confirmed cases living in rooms across from each other [11]. Given that most hotel ventilation systems are not designed for quarantine purposes and may not be easily renovated to increase air supply or install higher-grade filters, it is necessary to apply air cleaning technologies to provide an additional equivalent air exchange rate for the guest rooms and corridors [6].

Air treatment with filtration, in-room air cleaners, and germicidal ultraviolet (GUV) systems are recognized by the CDC as effective ventilation measures for mitigating the spread of viral aerosols [12], providing ventilation-equivalent benefits. Among these, portable air cleaners (PACs) equipped with a high-efficiency particulate air (HEPA) filter have emerged as cost-effective solutions for reducing indoor particulate air pollution and airborne viruses. Field studies conducted in homes with confirmed COVID-19 cases showed that PACs equipped with HEPA filters reduced mean $PM_{2.5}$ and PM_{10} concentrations by 78.8 % and 60.4 %, respectively, in primary rooms (i.e., where PACs were placed) and by 57.9 % and 60.4 %, respectively, in secondary rooms [13].

Advances in filtration technology have further enhanced air cleaning efficiency. For instance, Sheraz et al. developed a CuBTC/TiO_2/PS-based nanofiber electrospun on a HEPA filter, achieving a filtration efficiency of up to 99.82 % for $PM_{2.5}$, with negligible pressure drop compared to conventional HEPA filters [14]. The COVID-19 pandemic has also led to an increased interest in GUV technologies, particularly Far-UVC light. This spectrum offers high effectiveness in microbial inactivation while minimizing potential health risks due to its absorption by the tear layer of the eye or the stratum corneum of the skin [15]. Buonanno et al. [16] demonstrated that Far-UVC light reduced aerosolized murine norovirus (MNV), a conservative surrogate for airborne viruses such as influenza and coronavirus, by 99.8 % (95 % CI: 98.2–99.9 %) in an occupied room, while maintaining UVC doses within regulatory safety limits. Additionally, integrated air cleaning systems have been the focus of some studies. A recent study investigated an air cleaning prototype combining MERV-8 and MERV-13 fiber filters, an aluminum mesh filter, and UVC lamps in a poultry room [17]. The device achieved reductions of 55 % in total suspended particles and 47 % in total viable bacteria on average during a 28-day experiment.

Numerical methods are valuable and widely used tools to simulate airflows and the spread of airborne contaminants, taking into account the complexities related to aerosol transmission and the impacts of ventilation and air cleaning technologies affected by indoor airflow patterns. However, the multi-zone modeling method offers several advantages, especially for aerosol transmission across the rooms on a hotel floor. It can efficiently incorporate airflow through leakages, ventilation and filtration via mechanical systems, and dispersion of airborne contaminants across the entire building, taking into account various influential factors, including the generation and removal of airborne contaminants, door and window openings, occupancy schedules, and dynamic outdoor weather conditions [18]. Accordingly, multizone modeling has been applied to evaluate ventilation and infection risk by aerosol transmission for buildings [11,19–21]. For example, Yan et al. [21] investigated various mitigation strategies to mitigate SARS-CoV-2 transmission, evaluating the effectiveness of outdoor air ventilation, in-duct filtration and GUV, and in-room filtration unit and GUV. This study focused on US Department of Energy prototype models of different building types, including medium and large offices, standalone retail spaces, secondary schools, and small hotels. To date, there is a lack of systematic investigation providing effective and feasible air cleaning solutions for an entire floor of a quarantine hotel where HVAC system innovation is not possible, considering inter-zonal transmission via the aerosol route.

This study aimed to identify effective and feasible air cleaning solutions for quarantine hotels to minimize aerosol transmission risk. We developed a comprehensive multi-zone model using CONTAM for a floor of a hotel located in Baltimore, Maryland, which served as a quarantine facility during the COVID-19 pandemic. This model helped identify critical locations for aerosol transmission, enabling targeted interventions. We simulated the spread of viral aerosols on the floor and evaluated the performance of various mitigation strategies, comprising HEPA air cleaners, GUV fixtures, and air curtains, both individually and in combination. We proposed practical combined strategies, called air hygiene I and II, designed based on resource limitations, such as energy use, costs, space constraints, and noise generation. While air hygiene I focused on air cleaning in individual rooms, air hygiene II addressed air cleaning in both individual rooms and the common room (a gathering space). Additionally, we analyzed infectious exposure occupants received in different locations to assess their relative intensities in infecting occupants accurately.

2. Methodology

This section provides details on the studied hotel floor, field measurements, multi-zone modeling, air cleaning strategies and simulation details.

2.1. Description of quarantine hotel floor

For this study, we used the entire floor of a hotel located in Baltimore, MD, which was used in a cohort study to examine influenza transmission in the springs of 2023 and 2024 [22]. The hotel was also assigned as a quarantine facility during the COVID-19 pandemic. Fig. 1 shows the floor map. The "U-shaped" floor included 18 rooms for guests, 10 rooms for staff, and a common room for the guests' gathering during the daytime. The rooms marked in yellow on the layout were marginal spaces like the storage room and electrical room. This floor had an area of 1280 m^2, with ceiling heights of 2.4 m for the rooms and 2.7 m for the corridors. Notably, the common room had a volume of 91 m^3.

The whole floor was ventilated with a centralized system with two air supply diffusers in the middle of the long corridors. According to our measurements, each diffuser supplied outdoor air at a rate of approximately 950 m^3/h. The exhaust fans in the attached bathroom within each guest room exhausted air at a rate of 3 m^3/h. Each guest room had an air-conditioning system with a built-in fan-coil unit, which could only recirculate air to adjust indoor temperature. Their airflow was 600 m^3/h in the common room and 450 m^3/h in other rooms. It is essential to highlight that all windows on the floor were fixed and non-operable.

Each guest, including the index case releasing viral aerosols, was isolated while they were in their assigned rooms. To minimize cross-contamination during isolation, an effective air cleaning solution was necessary, as renovating the existing hotel HVAC system was not feasible. As a result, we aimed to design an effective quarantine environment using HEPA air cleaners, 222-nm GUV fixtures, and air curtains as air cleaning measures across the entire floor. This setup aimed to minimize airborne transmission outside the common room, which was the only area where guests interacted. By analyzing infection risk in the common room, we evaluated the effectiveness of these air cleaning measures in reducing within-room airborne transmission.

2.2. Field measurements

We performed two field experiments on the quarantine hotel floor. One experiment aimed to determine the number and operation mode of HEPA air cleaners in the common room, and another was intended to collect CO_2 concentration and differential pressure data for multizone model calibration. The detailed methodology of these experiments is provided in Appendix A.

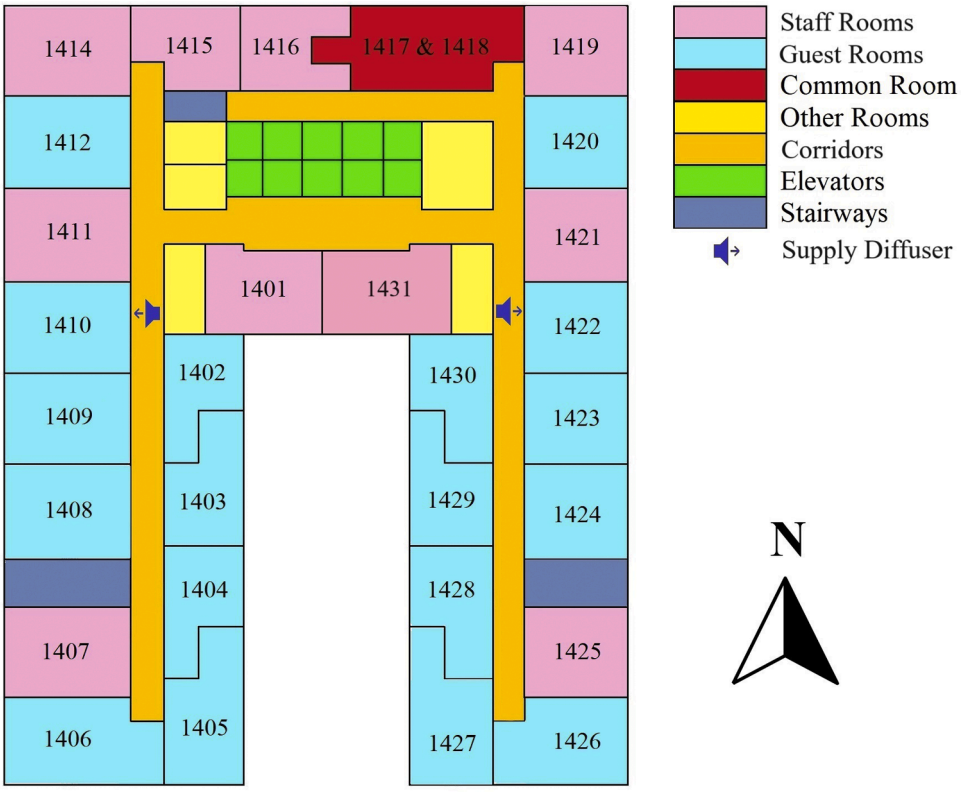

Fig. 1. Layout of the quarantine floor.

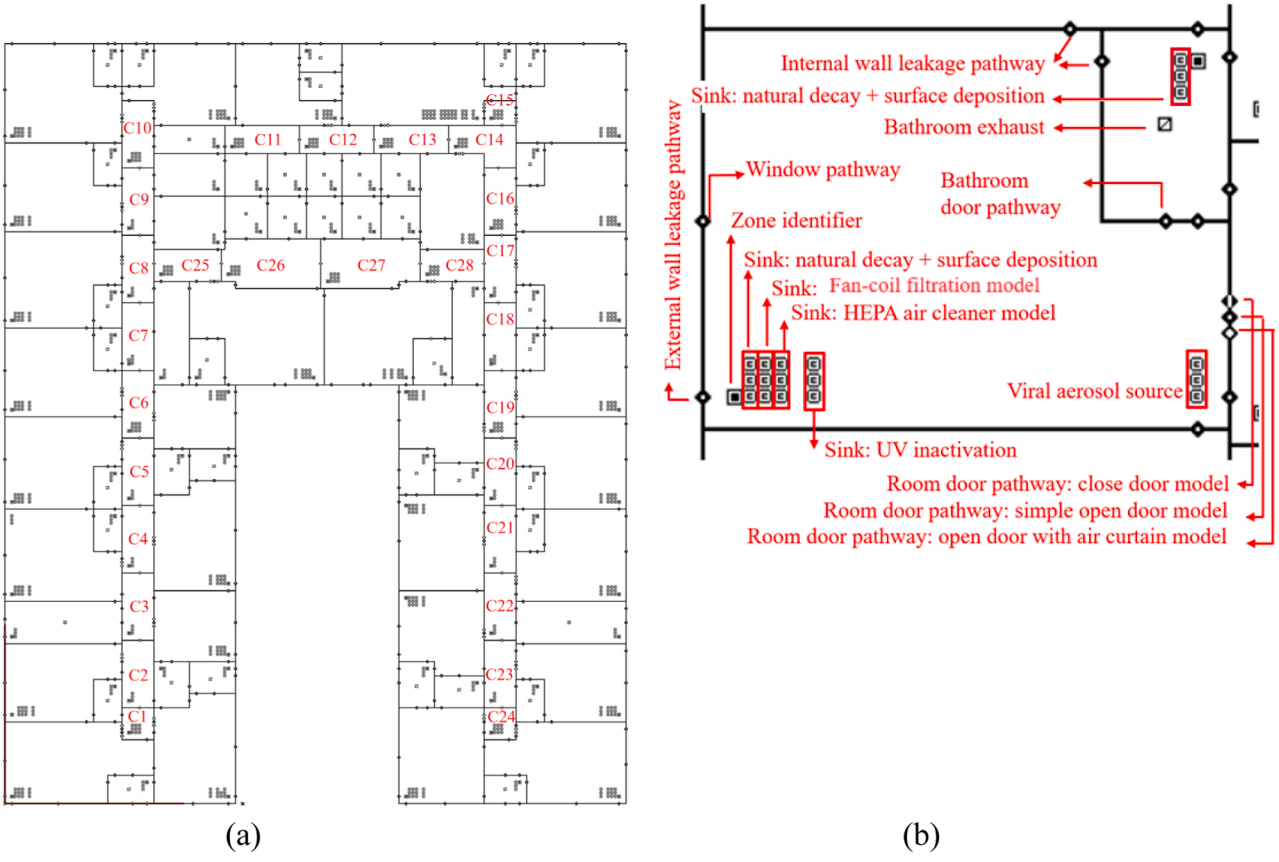

Fig. 2. Multi-zone model of the studied floor. The zones labeled C1-C28 represent the individual segments into which the corridor was divided.

2.3. Multi-zone modeling

2.3.1. Geometry representation and airflow paths

We utilized CONTAM software 3.4.0.4 [18] to develop a multi-zone model for simulating airflow and contaminant dispersion on the floor. The model was based on the actual floor plan and the airflows of mechanical systems determined by measurements. As shown in Fig. 2, this model incorporated building geometry representation, infiltration airflow paths, mechanical system airflow paths, and contaminant sources and sinks. Each zone represented a room or a corridor segment. Note that to model the viral aerosol spread accurately, we divided the corridor into small segments with lengths approximately equal to the room widths.

For different airflow paths, we employed leakage areas, as listed in Table 1. Two types of airflow paths were used for window and door openings: (1) a weather-stripped set for the common room to create controlled low ventilation conditions in this room, allowing us to focus only on the impacts of HEPA air cleaners and GUV fixtures on the transmission risk, and (2) a not weather-stripped set for other rooms. Air infiltration through windows, closed doors, and walls was computed using the leakage area model [18]. To account for the two-way flow through an open door interface -when the door was not equipped with an air curtain- as well as the interface between corridor segments, we used the single large opening model [18]. For doors with operating air curtains, the airflow path was modeled using a volume airflow-differential pressure (Q vs P) fit model, as detailed in the next section. In fact, we defined three distinct types of airflow paths for the room doors, positioned next to each other, as illustrated in Fig. 2(b): closed door, simple open door, and open door with air curtain. The selection of these airflow path was guided by schedules and determined based on the specific strategy and analysis requirements.

Additionally, to determine the airflow rates through air supply grille diffusers in the corridor and exhaust grilles in the bathrooms, we measured air velocities using a Kanomax Anemometer 6501–0E at 60 and 12 uniformly distributed points on the diffuser surface, respectively. At each point, the measurement was recorded for 10 ss at 1-second intervals, and the average velocity was taken as the representative value. Airflow rates were then calculated by multiplying the diffuser's average air velocity and the surface area. The used anemometer had an accuracy of ±2 % of the measured value or ±0.015 m/s, whichever was greater [23].

2.3.2. Modeling of viral aerosol source

Table 2 details assumptions related to the generation and removal of viral aerosols. In this study, we adopted the quantum concept proposed by Wells [29]. We assumed that the index case released aerosols containing SARS-CoV-2 at a quanta generation rate of 50 quanta/h [30]. Due to lack of clarity regarding the relationship between particle size and quanta generation rate, we applied the same quanta generation rate for the three particle size bins: 0.3–0.5 μm, 0.5–1 μm, and 1–5 μm [31,32].

Table 1
Leakage areas for different airflow paths in the multi-zone model.

Airflow elements	Leakage area	References
Closed door	330 cm^2/item	[24]
Common room door (closed)	15 cm^2/m^2	[25]
Bathroom door	330 cm^2/item	[24]
Elevator door	48.4 cm^2/item	[26]
Window	2.5 cm^2/m	[27]
Common room window	0.5 cm^2/m^2	[25]
Internal wall	2.25 cm^2/m^2	[28]
External wall	0.6 cm^2/m^2	[28]
Elevator wall	2.25 cm^2/m^2	[28]

Table 2
Input parameters for viral aerosol transmission simulation.

Inputs		Parameters	References
Quanta generation rate (quanta/h)		50	[30]
Breathing rate (l/min)	In rooms	8	[33,34]
	In corridor	14	
Particle deposition rate (1/h)	0.3–0.5 μm	0.74	[35]
	0.5–1 μm	1.1	
	1–5 μm	2.7	
Natural deactivation rate (1/h)		0.6	[36]
UVG deactivation rate (1/h)	Rooms	5.4	
	Corridor segments	16	
MERV-8 filter efficiency	0.3–0.5 μm	10 %	[35]
	0.5–1 μm	24 %	
	1–5 μm	70 %	
MERV-13 filter efficiency	0.3–0.5 μm	50 %	[35]
	0.5–1 μm	75 %	
	1–5 μm	97 %	
Air cleaner CADR (m^3/h)	2nd fan speed	202	
	3rd fan speed	298	
	4th fan speed	416	[37]

2.3.3. Modeling of air cleaning systems

Three air cleaning systems were considered for mitigating airborne transmission on the quarantine floor, including HEPA air cleaners, GUV fixtures, and air curtains (Fig. B.1). Each system employs a specific mechanism to reduce aerosol transmission risk. HEPA air cleaner physically captures aerosols containing viruses; GUV light inactivates viruses by disrupting their DNA or RNA [38], and the air curtain creates an air barrier at the doorway, limiting the movement of virus-laden aerosols from the rooms to the corridor when opening the doors. The detailed methodology for modeling these systems is provided in Appendix B.

2.4. Air cleaning strategies

We investigated a total of eight cases to evaluate the effectiveness of different air cleaning strategies for hotel floor quarantine. The deployment of the air cleaning systems is illustrated in Table 3 and Fig. C.1 (in the Appendix C). The eight cases are categorized as follows:

(1) Case 1 presented the baseline model without any air cleaning systems. It featured only MERV-8 filtration in the built-in fan-coil units within the rooms. This model was also used for multi-zone calibration.
(2) Cases 2, 3, and 4 examined the strategies involving individual air cleaning systems: air curtains, HEAP air cleaners, and GUV fixtures, respectively. In case 2, an air curtain strategy was implemented with an air curtain installed at each room door. Case 3 used a HEPA strategy. HEPA air cleaners were placed in all rooms, at corridor midpoints and ends, and in front of the common room and elevators. The common room, as discussed in Section 3.2.3, could be a significant source of viral aerosol release due to its low ventilation rate and specific airflow patterns, while the elevators could contribute to vertical airborne transmission to other floors. Case 4 employed a GUV strategy, replacing the HEPA air cleaners from Case 3 with GUV fixtures.
(3) Cases 5 and 6 explored the strategies using combined air cleaning systems. Case 5 was the HEPA + Air-curtain strategy, combining HEPA air cleaners and air curtains, merging cases 2 and 3. Case 6 was the HEPA + Air-curtain + GUV model, which further incorporated GUV fixtures, representing a combination of cases 2, 3, and 4.
(4) Case 7 presented the air hygiene I strategy (focused on individual rooms). It realistically incorporated layers of air cleaning systems for the quarantine floor, while considering constraints such as

Table 3
Number of air cleaning systems deployed for different strategies.

Air cleaning strategies	Air cleaning systems							
	Air curtain		HEPA air cleaner			GUV fixture		
	Common room	Guest/ staff rooms	Common room	Guest/ staff rooms	Corridors	Common room	Guest/ staff rooms	Corridors
Case 1: Baseline	–	–	–	–	–	–	–	–
Case 2: Air curtain	2	29	–	–	–	–	–	–
Case 3: HEPA	–	–	5	29	15	–	–	–
Case 4: GUV	–	–	–	–	–	4	29	15
Case 5: HEPA + air curtain	2	29	5	29	15	–	–	–
Case 6: HEPA + air curtain + GUV	2	29	5	29	15	4	29	15
Case 7: Air hygiene I	–	18	–	31	10	–	5	7
Case 8: Air hygiene II	–	18	5	31	10	4	5	7

space limitations, obstructions, safety concerns, and cost-effectiveness, along with this study's objectives. Firstly, air curtains were installed only for the rooms where feasible. In some rooms, the space between the top of the door frame and the corridor ceiling was too narrow to install air curtains. Secondly, GUV fixtures were installed only in the corridor and certain staff rooms where there was a specific concern about infection risk. The limited use of GUV was intended to avoid potential tripping hazards, as these systems featured tripods and cables. It also aimed to reduce costs, as GUV fixtures were significantly more expensive than HEPA air cleaners and air curtains (6 to 10 times more expensive). Retrofitting these fixtures in the rooms without tripods and cables was also not easily possible. Thirdly, as one of the objectives of the study, no air cleaning system was assigned to the common room in this model. This allowed for the investigation of aerosol transmission without interference. Finally, all bathroom exhausts were assumed to be covered with a MERV-16 filter to minimize vertical infection transmission through exhaust systems.

(5) Case 8 introduced the air hygiene II strategy (addressing both individual rooms and the common room). This model was similar to the air hygiene I strategy with only one difference: using HEPA air cleaners and GUV fixtures in the common room to further control aerosol transmission in this critical room. According to the results of the field experiments as described in section A.1 (Appendix), five HEPA air cleaners were added to the common room and assumed to run at the 2nd fan speed. In addition, four GUV fixtures were added to meet the equivalent air exchange rate (eACH) requirement specified in the HVAC Design Manual for Hospitals and Clinics [39] for operating/surgical rooms (20 1/h).

2.5. Simulation methods

We conducted the simulations in both steady and transient states to characterize airborne transmission patterns within the quarantine floor. The simulations were also used to evaluate the performance of air cleaning strategies in minimizing airborne transmission. Table 4 lists different air cleaning strategies analyzed in the steady-state and transient simulations.

2.5.1. Steady-state simulation

Steady-state simulation was used for three specific applications. One was to evaluate the improvement in the performance of an air curtain by adding a MERV-13 filter to its intake grill. We then analyzed the zonal dispersion patterns of contaminants across the floor to help develop air cleaning strategies systematically. Another was to assess the performance of different air cleaning strategies in reducing inter-zonal transmission on the quarantine floor.

2.5.1.1. Method for evaluating the impacts of air curtain with filtration. To evaluate the performance of the air curtain while the source was in the corridor, we set the viral aerosol source in the corridor segment between rooms 1405 and 1406 (indicated by a star in Fig. 7). We simulated the spread of quanta concentration with and without MERV-13 filter on air curtain's intake grill. We evaluated the impact of the MERV-13 filter by comparing the steady-state quanta concentration levels in rooms 1405 and 1406.

2.5.1.2. Method for evaluating air cleaning strategies. To evaluate the performance of air cleaning strategies in reducing inter-zonal airborne transmission independently of the source location, we placed the index case in each potential location, one at a time. We then examined the integrated effects of sources and sinks [19]. To do this, for each air cleaning strategy, we developed 19 separate multi-zone models, each with the index case located in a different guest room or the common room. After performing simulations, to exclusively analyze the inter-zonal transmission, we excluded the quanta concentration in the source location from each model's analysis by considering a zero quanta concentration in the source location. This way, we could focus on the viral aerosol release to other areas. It also allowed to treat all three air cleaning systems without bias, as air curtains do not affect the source location's quanta concentration, unlike HEPA air cleaners and GUV fixtures. Then, for each individual zone, we calculated the average quanta concentration across all 19 models. Finally, we computed the volume-weighted average of the quanta concentration throughout the whole floor. This provided a single value representing the overall quarantine performance corresponding to each strategy.

To assess the reduction in inter-zonal transmission, we defined a new index, called inter-zonal air exchange rate (zACH), by adapting the existing eACH formula [40]. This index quantifies the effectiveness of air cleaning strategies in reducing inter-zonal transmission from the index

Table 4
Air cleaning strategies analyzed in steady-state and transient simulations.

Simulation type	Air cleaning strategies							
	Case 1: Baseline	Case 2: Air curtain	Case 3: HEPA	Case 4: GUV	Case 5: HEPA + air curtain	Case 6: HEPA + air curtain + GUV	Case 7: Air hygiene I	Case 8: Air hygiene II
Steady-state	✓	✓	✓	✓	–	–	✓	✓
Transient	✓	✓	✓	✓	✓	✓	✓	✓

case's zone to other zones, making it a crucial parameter for quarantine facilities. Please note that zACH measures the overall effectiveness of all air cleaning systems of the same type across the entire floor.

To develop the zACH, we defined the parameters of the eACH formula in a novel way to align with our objective of examining inter-zonal airborne transmission. The zACH was calculated as follows:

$$zACH = \frac{G_e}{C_{ss}V} - \frac{Q}{V} \quad (1)$$

where, C_{ss} is the volume-weighted average of the quanta concentration throughout the floor (quanta/m^3). This parameter is derived by averaging quanta concentrations across different individual models, each with the index case located in a potential position. The quanta concentrations at the source locations were excluded from the models. V is the volume of the floor (m^3), and Q is the rate of the outdoor airflow entering the floor. The equivalent quanta generation rate, G_e (quanta/h), was calculated through:

$$G_e = QC_{ss,b} \quad (2)$$

where $C_{ss,b}$ represents the volume-weighted average quanta concentration (quanta/m^3) in a model without air cleaning systems and fan-coil filtration. This parameter is derived by averaging quanta concentrations across different individual models, each with the index case located in a potential position. The quanta concentrations at the source location were excluded from the models. The detailed calculation steps of zACH are provided in Appendix D.

During these simulations, all doors were kept open to simulate a worst-case scenario. The ambient wind was excluded from the simulations. The room and corridor temperatures were set to 22 °C and 24 °C, respectively, based on our measurements. Outdoor temperature was assumed to be 7 °C, the average temperature from March 1st to March 4th, 2023, at the Baltimore/Washington International Airport Station [41]. Taking advantage of multi-zone modeling of the entire building, as discussed in Section 2.5.2.1, we applied the average airflow rate entering or exiting each elevator shaft and staircase as the boundary condition.

2.5.2. Methodology for transient simulations

Following the initial steady-state simulations, we conducted transient simulations to assess the viral aerosol transmission risk and evaluate the effectiveness of various air cleaning strategies in detail. These simulations also helped us incorporate dynamic weather conditions and occupant movements to provide a more realistic representation of the quarantine.

After transient simulations, we processed the data to assess the infectious exposure and infection risk. We calculated the dose of viral aerosols inhaled by occupants during the entire exposure period (infectious exposure), D (quanta), using the following equation [42]:

$$D = \sum C(t).p.\Delta t \quad (3)$$

in which, C is the quanta concentration in the zone where the occupant is located (quanta/m^3), p represents the breathing rate (m^3/min), and Δt represents the simulation time step (min). We then calculated the infection risk, P, through the Wells-Riley model [21]:

$$P = 1 - \exp(-D) \quad (4)$$

In the transient simulations, we placed the index case in the room identified to have the highest possibility to cause inter-zonal transmission to an adjacent room. Each simulation ran for a duration of 72 h, starting at 20:00 on March 1, 2023, and ending at 20:00 on March 4, 2023. Throughout the simulation period, we maintained an indoor temperature of 22 °C for rooms, and 24 °C for corridors.

We considered a total population of 28 individuals, including 18 guests and ten staff members. Each guest was assigned to a separate guest room, while each staff member was allocated to a dedicated staff room. The staff were supposed to stay consistently in their own rooms throughout the simulation. However, for guests, we developed a specific movement schedule, as illustrated in Fig. 3, based on the schedule of the cohort study. We assumed that guests spent 5 min in the corridors when walking between the common room and their individual rooms. To model the movement of the index case along the corridor, the source was considered to move sequentially between corridor segments along the route between their room and the common room. As the worst-case scenario, we assumed that the guest residing in room 1405, located across from the index case room, walked within the same corridor zone simultaneously with the index case. The common room doors were kept open for 5 min while guests were in the corridor. Other room doors remained open for 1 min when guests entered or exited their rooms, as well as during meal deliveries at 8:00, 14:00, and 17:00 each day.

Recognizing the significance of installation costs and energy consumption considerations for decision-makers [43–45], we evaluated both the energy consumption over the entire simulation period and installation costs of the strategies.

Energy consumption of each system was calculated by multiplying the device power with its operational time. To gather the power data, we used a HOBO Plug Load Data Logger while each system ran for 10 min with 1-minute time intervals. We then calculated the average value. For the HEPA air cleaner, power data was measured for all fan speed modes. We then calculated the total energy use for each strategy by accumulating the energy consumption of the involved systems based on Table 3. Additionally, the power density (W/m^2) for each strategy was computed by dividing the total power consumption by the hotel floor area.

Installation costs were also estimated by summing the prices of all devices involved in each strategy. The device prices were obtained from the manufacturers' websites. It is $255 for air curtain [46], $429 for each HEPA air cleaner [37], and $2500 for each GUV fixture [47].

2.5.2.1. Boundary conditions for transient simulation analysis.

To account for the variability in weather conditions, we created and employed a weather file based on climate data obtained from the Weather Underground repository for the Baltimore/Washington International Airport Station [41]. The variations in key weather parameters are illustrated in Fig. 4.

To take into account the dynamic airflow rates associated with elevator shafts and stairwells, we created a multi-zone model for the entire building. We copied the model of the 14th floor to other floors. For the lobby, we removed the rooms and incorporated the infiltration through two revolving doors located on the west side of the lobby using the following equation [48]:

$$Q = 1.6\Delta P^{0.66} \quad (5)$$

where, ΔP is the pressure difference across the door (Pa). We then simulated the multi-zone model for the entire building to capture the airflow rates to/from the shafts. The extracted airflow rate data were used in the multi-zone model of the quarantine floor, serving as boundary conditions for elevator shafts and stairwells.

We also calculated the temporal variation of the neutral pressure level (NPL) height over a one-month period, from January 30 to February 29, 2024. The NPL is defined as the height where the indoor and outdoor pressures are equal. The NPL was assessed at the north wall due to its relevance to airflow patterns in the common room.

3. Results

This section presents the results of field measurements and model calibration, steady-state simulations, and transient simulations. With field measurements, we determined the optimal deployment of HEPA air cleaners in the common room, balancing acoustic comfort and air cleaning requirement. Moreover, we calibrated the multi-zone model for

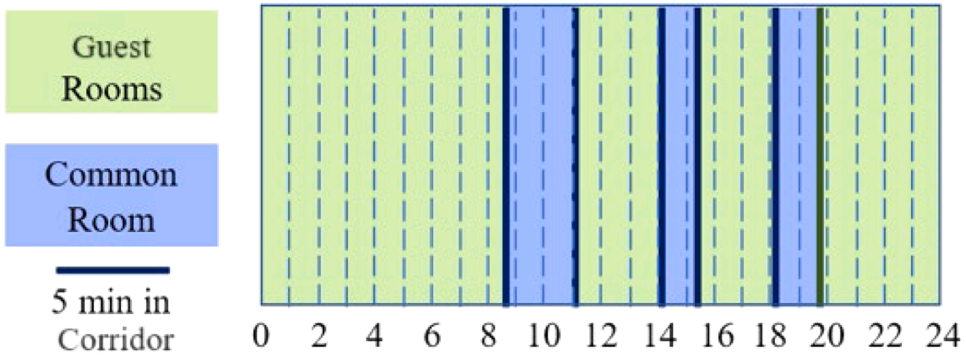

Fig. 3. Daily schedule for the guests.

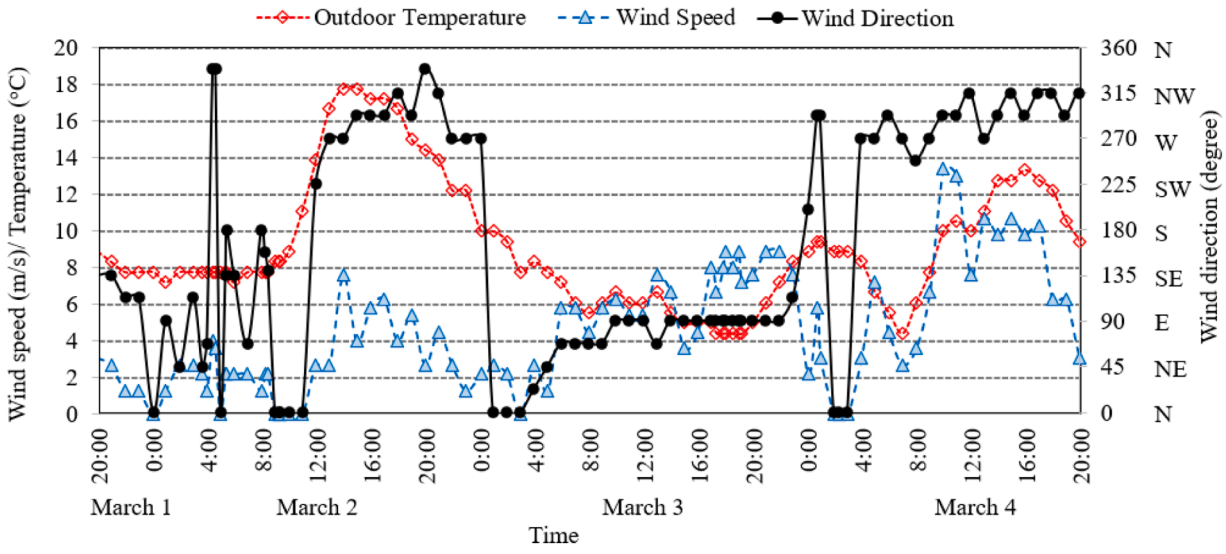

Fig. 4. Weather parameter variations for Baltimore (March 1 to March 4) used in simulations.

the quarantine floor with experimental data. Steady-state simulations helped us develop the model systematically and design the air cleaning strategies based on the identified areas prone to contaminant concentration build-up. They also helped quantify the effectiveness of air cleaning systems in reducing inter-zonal airborne transmission across the rooms. However, steady-state simulations could not easily account for influential dynamic factors such as wind conditions and the movement of the index case in the corridor. Thus, we conducted transient simulations to account for these factors, providing a more realistic and detailed representation of the quarantine study. This way, we could consider different possibilities for airborne transmission on the floor beyond just inter-zonal transmission from the index case room, which was evaluated in the steady-state simulations. Using transient simulations, we could also accurately calculate the infectious exposure occupants receive in different locations to assess their relative intensities.

3.1. Experimental results and model calibration

This section provides the results of field experiments and model calibration.

3.1.1. Noise level and eACH for HEPA air cleaners

At a background noise level of 30 dBA, the noise level of a single HEPA air cleaner was 33 dBA, 40 dBA, 49 dBA, and 55 dBA when running at 1st, 2nd, 3rd, and 4th fan speed modes, respectively. These results indicate significant increases in the noise level with higher fan speeds. Accordingly, to ensure a quiet sleeping environment, the HEPA air cleaners were set to the 2nd fan speed mode in guest rooms. In other spaces (except for the common room), they were set to the 4th fan speed mode. During our search for a quiet HEPA air cleaner, we found that these values were typical for HEPA air cleaners, regardless of the manufacturer.

Fig. 5 summarizes experimental results on noise levels and eACH when using multiple HEPA air cleaners in the common room. The background noise level, measured without the HEPA air cleaners running, was 42 dBA. All three scenarios met the eACH requirement, based on the ASHRAE 62.1 Standard [49] recommendation for "Physical therapy exercise areas" (10 1/h). However, the noise level was lowest at 50 dBA in the scenario with 5 HEPA air cleaners because noise level does not increase linearly with the number of devices. Consequently, using 5 HEPA air cleaners (i.e., more units) operating at the 2nd fan speed mode (i.e., lower fan speed mode) effectively balances air cleaning performance and noise generation. Thus, this scenario was selected for the common room.

3.1.2. Model calibration

As the speed of the axial window fan in room 1431 increased (Fig. 6 (a)), the differential pressure between this room and the corridor rose. This is because, at higher speeds, the fan enhanced airflow from the outside into the room, which creates a higher internal pressure relative to the corridor.

We also calculated the ACH to be 0.46 ± 0.022 1/h in the common room and 1.4 ± 0.19 1/h in room 1405. With the strict control over the ventilation conditions (using weather-stripped doors and windows), the

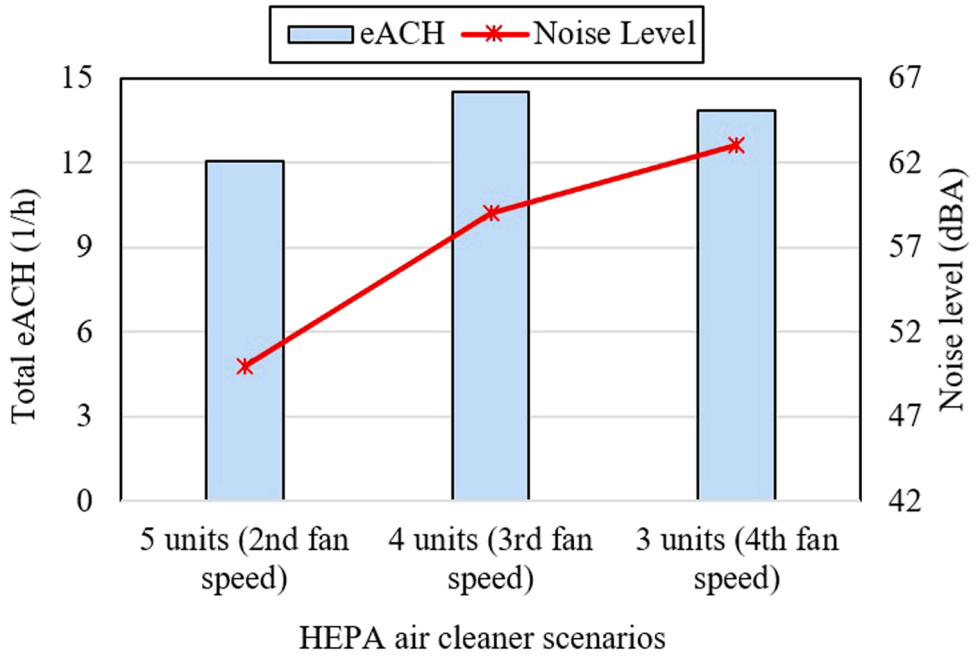

Fig. 5. Comparison of noise level and eACH for HEPA air cleaner scenarios for the common room.

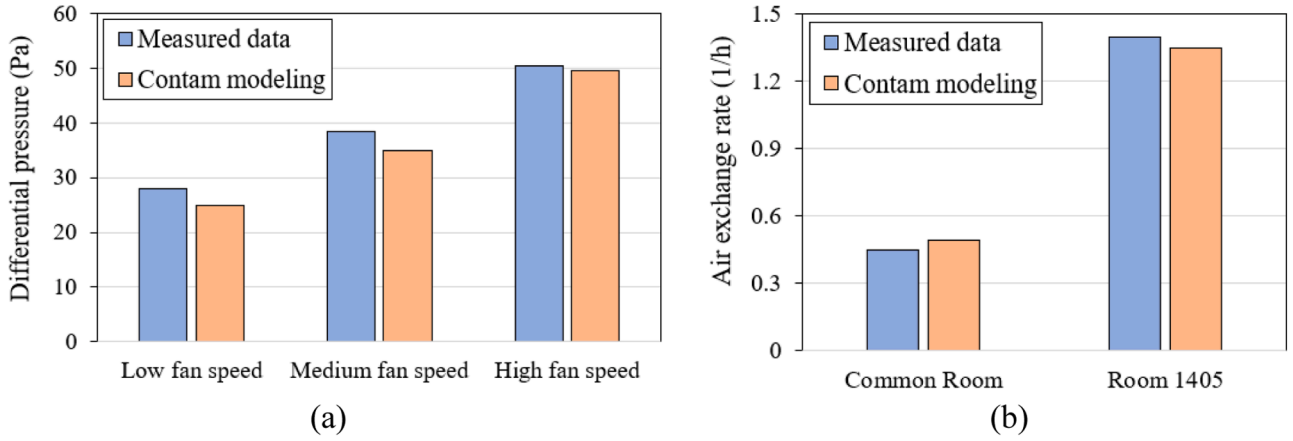

Fig. 6. Comparison of measured and model-calculated data.

impact of outdoor weather variations on ventilation was minimized in the common room, resulting in a significantly lower standard deviation of ACH compared to room 1405 (with not weather-stripped airflow paths).

Fig. 6 validated the multizone model by comparing the measured and simulated data in terms of differential pressure between room 1431 and corridor, as well as the average ACH in the common room and room 1405. The differences between the experimental and simulated were within ±10 % of the measured data for both sets of experiments, indicating a good agreement between model predictions and the experimental data.

3.2. Steady-state simulation results

This section presents the improvement in air curtain performance with the addition of a MERV-13 filter, the zonal distribution of contaminants across the floor, and the effectiveness of air cleaning strategies in reducing inter-zonal airborne transmission.

3.2.1. Enhanced air curtain performance with MERV-13 filtration

When the index case was placed in the corridor segment at the end of the corridor, the contaminants spread primarily to the rooms and their associated bathrooms at the corridor's end (Fig. 7). This was due to the specific airflow patterns and the direction of the airflows, which limited the dispersion of contaminants along the corridor. As shown in this figure, adding MERV-13 filter to the air curtain intake grille resulted in a 56 % reduction in average quanta concentrations in the zones surrounding the index case located in the corridor. Therefore, this modification transforms air curtains into valuable control systems for room protection. Accordingly, we incorporated the MERV-13 filtered air curtain model in our subsequent simulations.

3.2.2. Impact of air hygiene I strategy on zonal distribution of quanta concentration

Fig. 8 compares the average quanta concentration for the baseline and air hygiene I strategies. In the air hygiene I strategy, the average concentration was reduced in almost all zones throughout the floor, with a maximum reduction of 99 %.

In the absence of additional air cleaning systems (Fig. 8a), quanta

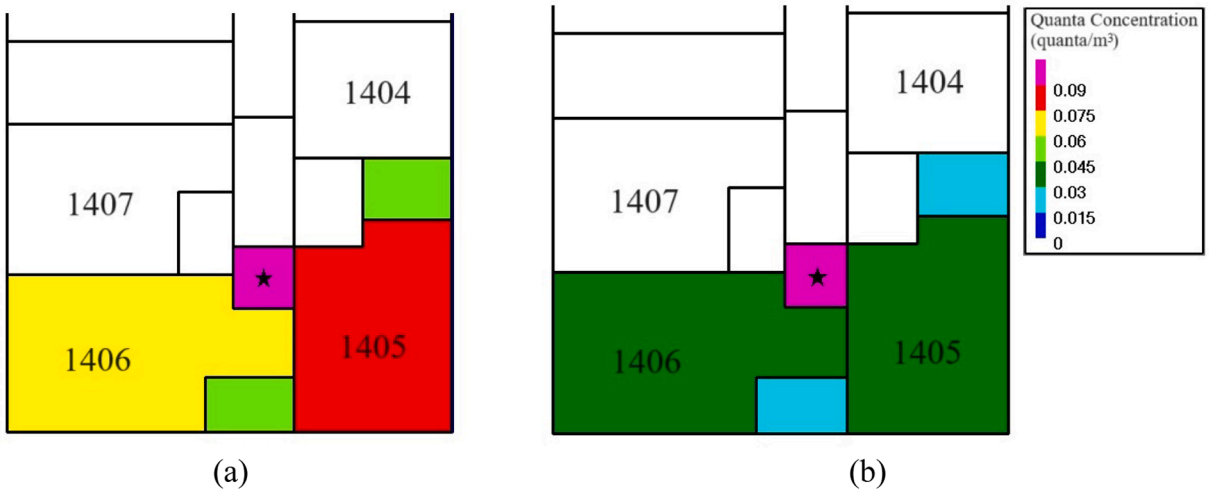

Fig. 7. Impact of applying MERV-13 filtration on air curtain performance. The star denotes index case. The standard air curtain refers to an air curtain without a filter.

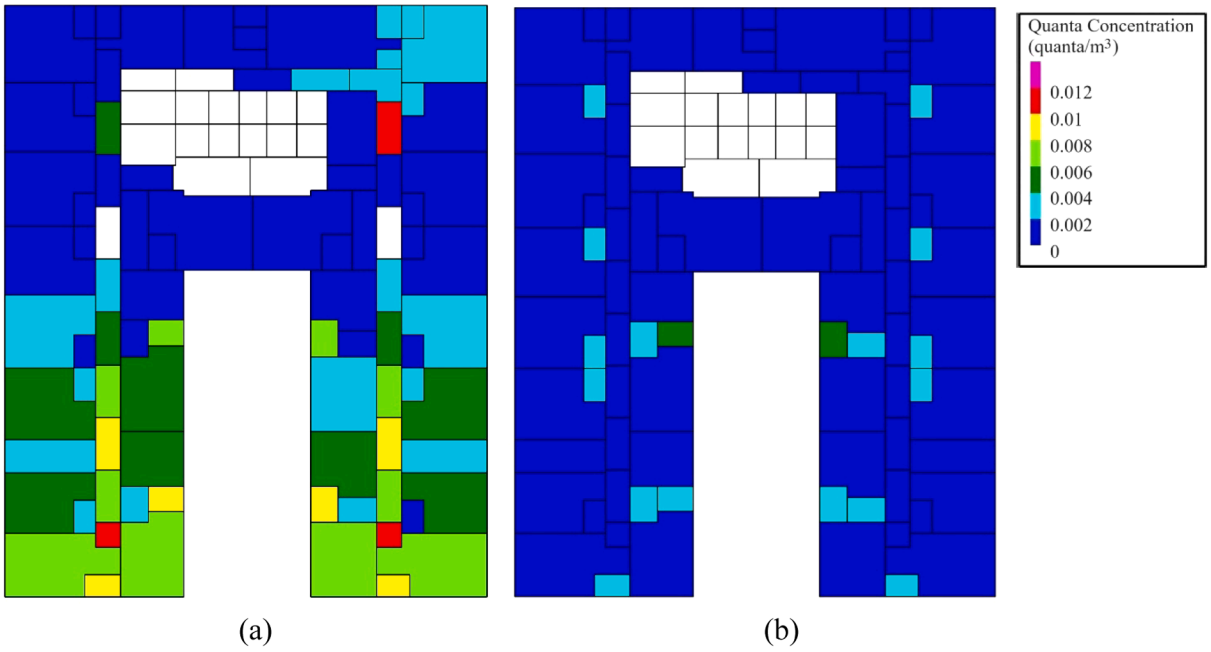

Fig. 8. Zonal distribution of average quanta concentration across the quarantine floor.

concentrations were higher in zones at the south ends of long corridors, showing a highest tendency for the accumulation of viral aerosols there. This was due to the airflow pattern and the location of guest rooms, which were potential index case locations, were mostly situated in the middle and southern sections of the corridors. Air supplied from the diffusers in the middle of long corridors moved towards the corridor ends, carrying viral aerosols released from the rooms into the corridor. Additionally, viral aerosols released at the ends of long corridors became trapped and infiltrated into nearby rooms through doorway airflows. These observations highlighted the importance of installing appropriate control measures at the ends of long corridors to mitigate aerosol transmission risk effectively.

3.2.3. *Comparative efficacy of air cleaning measures*

The power consumption and price details of air cleaning systems are presented in Table 5. The results indicate that the air curtain consumes significantly more electrical power compared to HEPA air cleaner and GUV fixture. However, it is important to note that the air curtain operates temporarily, unlike the continuous operation of the other two systems. Despite its high air cleaning performance, the GUV fixture consumes relatively low power.

Table 5
Power consumption of air cleaning systems.

Air cleaning system		Power use (W)
Air curtain		255
HEPA air cleaner	1st speed	4.0
	2nd speed	8.7
	3rd speed	20
	4th speed	36
GUV fixture		16

Table 6 presents both the overall zACH values for different air cleaning strategies. As can be seen, air curtains did not contribute to

Table 6
Air cleaning performance of different strategies in steady-state simulations.

Strategies	zACH (1/h)	Power density (W/m^2)	No. of devices	Attributed clean airflow rate per device (m^3/h) for inter-zonal transmission
Case 1: Baseline	0.4	1.38	30	40
Case 2: Air curtain*	1.7	6.18	31	156
Case 3: HEPA	2.8	0.89	49	179
Case 4: GUV	3.5	0.60	48	229
Case 7: Air hygiene I*	7.6	4.51	71	776
Case 8: Air hygiene II*	8.5	4.59	80	864

* In the real-world applications, air curtains operate intermittently, activating only when doors are open, unlike HEPA air cleaners and GUV fixtures, which may run continuously. Therefore, these values should not be used for direct comparisons between different control measures. Instead, they serve as estimates for installed capacity requirements.

reducing viral aerosol concentration at the index case location. The GUV strategy showed the highest zACH for the entire floor (a total of 3.5 1/h of clean air), followed by the HEPA strategy (a total of 2.8 1/h of clean air).

We also calculated the attributed clean airflow rate per device for each air cleaning system. As expected, GUV fixture provides the highest attributed clean airflow rate to control inter-zonal transmission. It's important to note that the zACH and attributed clean airflow rate values correspond to our specific configuration of air cleaning measures and may be different for another configuration, although they provide a framework for performance comparison.

The results also show that the air curtain has a significantly higher power density compared to the other air cleaning systems. As a result, the air hygiene strategies I and II, which incorporate the air curtain, also exhibit relatively higher power densities.

As shown in Table 6, air hygiene I and II strategies effectively reduced inter-zonal transmission risk, achieving overall zACH values of 7.6 and 8.5 1/h of clean air, respectively. It shows that the air hygiene II strategy has a better performance in reducing inter-zonal transmission compared to air hygiene I strategy. As observed in Fig. 9, placing the index case in the common room led to the highest quanta concentrations in its nearby room due to the trapping of viral aerosols in the corridor segment between the common room and its adjacent room, i.e., room 1419. Therefore, adding HEPA air cleaners and GUV fixtures in the common room in the air hygiene II strategy significantly increased the zACH compared to the air hygiene I strategy.

The term "maximum steady-state quanta concentration in adjacent rooms" in Fig. 9 refers to the maximum quanta concentration in the rooms near the index case's location after the concentrations reached steady state. This parameter represents the worst-case scenario for inter-zonal transmission to other rooms for any potential location of the index case. For instance, when the index case was placed in room 1403, room 1408 exhibited the highest quanta concentration among all neighboring rooms. Consequently, the concentration in room 1408 was reported in this figure. When the index case was placed in the guest rooms at the ends of the two long corridors (i.e. Rooms 1405, 1406, 1426, and 1427), neighboring rooms experienced more significant viral aerosol concentrations compared to the scenarios with the index case situated in other guest rooms. This phenomenon underscored the importance of inter-zonal contamination from rooms located at corridor ends to those directly opposite when doors are simultaneously open. Based on this analysis, we selected room 1406 as the index case room for transient simulations, representing the worst-case scenario.

When the index case was located in Room 1420, the adjacent rooms experienced significantly lower concentrations of viral aerosols compared to other scenarios where the index case was placed in other locations. This outcome is primarily attributed to the main route of viral aerosol spread across the rooms, which is their transport from the index case's location to the corridor and subsequently to other areas via airflow. For the corridor segment in front of the Room 1420, the airflow pattern is unique: air movement from both directions converges toward this segment. Air supplied from the corridor diffuser on one side, coupled with infiltration from the elevator shafts and stairwells on the other side, effectively prevents the movement of air - and therefore, viral aerosols -from Room 1420 into the corridor and onward to other spaces. The negligible amount of viral aerosols observed in adjacent rooms is attributed to minor infiltration through common walls.

3.3. Transient simulation results

We first assessed the variations in the NPL of the building at the north

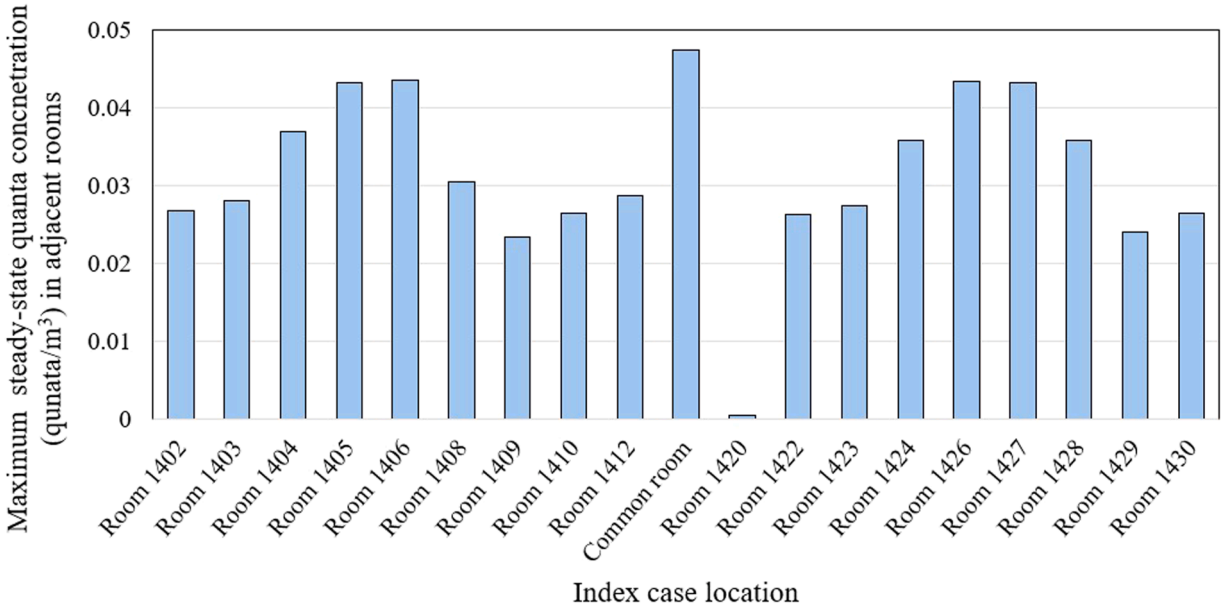

Fig. 9. Maximum steady-state quanta concentration in adjacent rooms for different index case locations in the baseline model.

wall to determine the direction of airflow through the external wall of the common room. Next, we presented the results of the infectious exposure inhaled by occupants and the airborne transmission risk considering dynamic weather conditions and the movement of the index case.

3.3.1. Building NPL variation

Fig. 10 illustrates the temporal NPL variation at the north side where the common room is located. The NPL fluctuated significantly with changing outdoor conditions between the Lobby and the 10th floor, consistently remaining below the building's mid-height (11th floor). As the quarantine study was conducted on 14th floor, indoor-outdoor pressure difference on the north side ensured a consistent airflow direction from the common room to the outdoor environment.

3.3.2. Temporal variation of quanta concentration

Fig. 11 illustrates the time-dependent variation in quanta concentration for room 1406 (the index case room) and the common room. As expected, concentrations increased while the index case was present in a room and declined exponentially after their departure.

In the baseline case (Fig. 11a), the quanta concentration in the index case room slightly decreased at 8:00, 13:00, and 15:00 when the door was opened for meal service, allowing viral aerosols to escape into the corridor. Notably, this concentration drop did not occur when using the air curtain strategy, indicating that air curtains were effective in minimizing the escape of viral aerosols from the room.

Unlike air curtains, HEPA air cleaners and GUV fixtures significantly reduced concentrations in both rooms. The concentration reduction was more pronounced in the common room due to the greater number of HEPA air cleaners and GUV fixtures installed there. The GUV system had a higher eACH than the HEPA air cleaner system running at the 2nd fan speed, resulting in a greater reduction in the steady-state quanta concentration.

3.3.3. Comparative analysis of air cleaning strategies

Fig. 12 illustrates the reduction in the maximum individual infectious exposure among healthy guests and staff compared to the baseline model. For all air cleaning strategies, the maximum individual infectious exposure was received by the guest in room 1405 and the staff member in room 1419 due to their proximity to the index case room and the common room, respectively. These maximum individual exposure values highlight the individuals at the highest risk of infection and provide valuable insights into the upper limits of infection risk across various locations and strategies. Fig. 12 also includes the installation cost and energy consumption associated with each strategy.

Staff are assumed to stay in their rooms throughout the analysis, but for the guests, we evaluated their inhaled exposure in three locations: guest rooms, corridors, and the common room. The exposure received in the guest rooms and corridors were used to assess the efficacy of air cleaning strategies in a quarantine facility, where aerosol transmission is undesirable, while the analysis of the common room demonstrated the effectiveness of the strategies in reducing within-room infection risk.

The air curtain strategy showed the least reduction in the maximum individual infectious exposure for both guests and staff across all locations. While air curtains effectively minimized the escape of viral aerosols from the rooms, they could not effectively control the source in the corridor, even with MERV-13 filter. Air curtains may increase the rate of airflow from the corridors into the rooms, which reduces the filtration impacts of MERV-13 filter if the index case is located in the corridor. It highlighted the necessity of using source control measures in quarantine facilities, which lower the contaminant concentration by nature. The advantage of air curtains is their low installation cost and energy consumption due to the limited operation time.

As shown in Fig. 12a, the GUV strategy outperformed the HEPA air cleaner strategy in protecting the guest in room 1405 from inter-zonal airborne transmission. However, the HEPA + air curtain strategy led to be a better performance than the GUV strategy. The HEPA + air curtain + GUV strategy achieved the greatest reductions in the maximum individual infectious exposure for all locations. However, the reduction in infectious exposure did not increase linearly with the number of deployed systems. While the HEPA + air curtain + GUV strategy had initial costs 2.9 and 2.3 times higher than air hygiene I and II strategies, respectively, and consumed 1.6 and 1.5 times more energy, it only achieved additional reductions in the maximum infectious exposure ranging from 5 to 18 % in the rooms compared to the baseline model, implying the need to balance air cleaning performance with installation costs and energy consumption considerations . Overall, strategies incorporating a large number of GUV fixtures are associated with significantly higher installation costs, while those utilizing HEPA air cleaners tend to have relatively higher energy consumption.

Since the common room was close to room 1419, where the staff member receiving the maximum individual infectious exposure stayed, transitioning from air hygiene I to air hygiene II also affected the exposure they received in their rooms. To reduce the infection risk of all occupants to below 1 % in their rooms, with a total exposure time of 54 h and 45 min, a reduction of at least 35 % in the infectious exposure was required for the guest in room 1405 and 73 % for the staff member in room 1419, compared to the baseline case. Accordingly, all strategies except the air curtain strategy could ensure a maximum 1 % infection risk in the rooms.

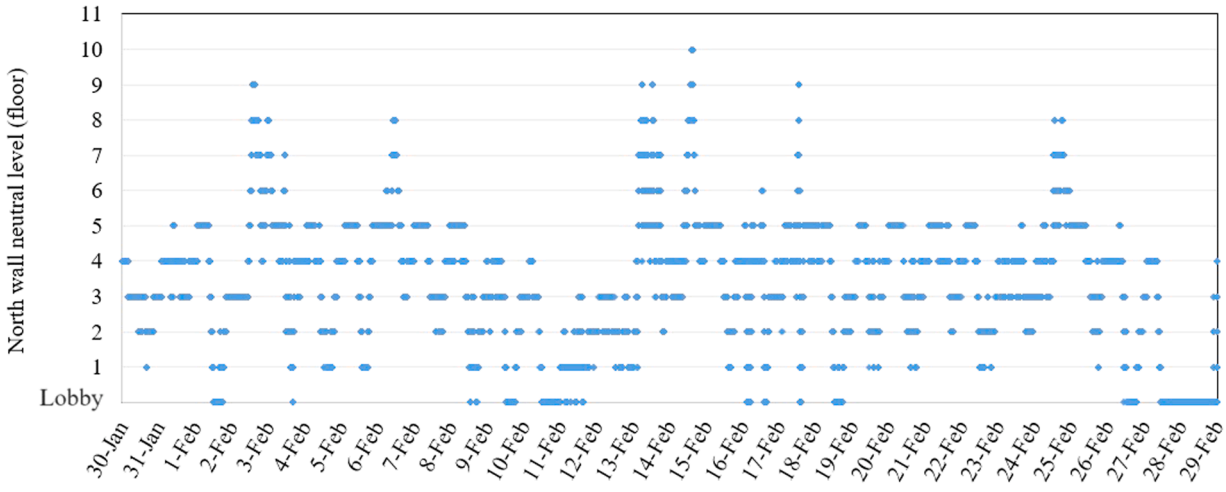

Fig. 10. Dynamic variation of NPL at the north wall.

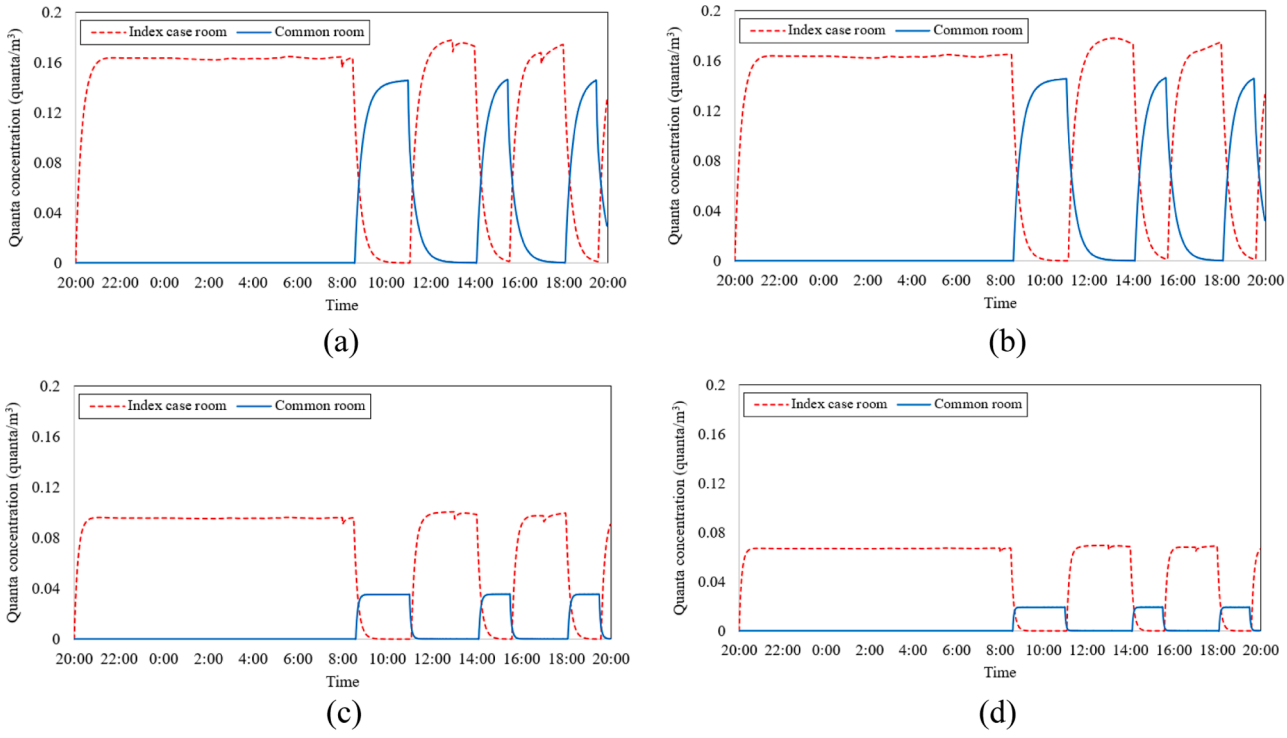

Fig. 11. 24-hour quanta concentration profiles in the index case room and the common room.

The maximum individual infectious exposure received by guests in the corridor decreased by 10–26 % for different air cleaning strategies (Fig. 12b), indicating the relatively lower effectiveness of these strategies in this area. This outcome can be attributed to several factors. First, clean air is directly discharged into the corridor, effectively diluting air contaminants and playing a dominant role in reducing contaminant concentrations. This overweighted the performance of air cleaning systems. Second, people in corridors were typically in motion, which helped disperse exhaled viruses and reduce their accumulation in areas with poor local ventilation. Third, the lower distribution density of air cleaning systems in the corridor contributed to the smaller reductions in the inhaled exposure. Despite the high airflow rate, a guest walking alongside the index case in the corridor faces a potential infection risk of 1.5–1.8 % across different air cleaning strategies (for a total exposure duration of 90 min). This suggests that even proximity to an index case in passageways, such as corridors, can lead to high risks of infection despite the use of air cleaning systems. As a result, in quarantine facilities, mask-wearing in corridors is highly recommended to minimize potential airborne transmission [50].

Fig. 12c shows the infectious exposure that guests received in the common room. The air curtain and air hygiene I strategies did not reduce the infectious exposure, as they did not provide source control for the common room. As expected, the greatest reduction in the infectious exposure was achieved with the HEPA + air curtain + GUV and air hygiene II strategies, both of which had the same air cleaning setup in this room.

For different air cleaning strategies, the guest in room 1405 received 84–98 % of their total infectious exposure (i.e. the cumulative exposure from all locations) in the common room, 1.8–13 % in the corridor, and 0.5–3.1 % in their own room, indicating that aerosol transmission is most likely to occur in the common room across all strategies.

Fig. 13 illustrates the average total infection risk for the guests and staff members, aggregated from all locations, under different air cleaning strategies. The strategies without source control measures posed significant infection risk for the guests. The HEPA + air curtain + GUV and air hygiene II strategies showed the lowest average infection risk. Infectious exposure was primarily received in the common room, resulting in a higher average infection risk for the guests compared to the staff. This highlighted the necessity of over-filtering in all meeting rooms and gathering places to minimize the infection risk.

4. Discussion

In this study, we evaluated the air cleaning effectiveness of different air cleaning strategies, comprising HEPA air cleaners, GUV fixtures, and filtered air curtains in reducing the infectious exposure of quarantine hotel occupants.

4.1. Feasibilities of the simulation methods

Outdoor weather conditions can drastically alter the direction and volume of infiltration to or from the floor of interest through stairwells and elevator shafts. Therefore, before simplifying a building's multi-zone model to focus on just one floor, it is essential to determine whether the dynamic outdoor environment significantly impacts the NPL. If such an impact exists, a multi-zone model for the entire building is necessary. In our study, the NPL varied significantly over time, necessitating the incorporation of shaft infiltration into the multi-zone model of the quarantine floor.

Using the one-floor model, we conducted simulations in both steady and transient states. Steady-state analyses allowed us to identify areas with a higher likelihood of cross-contamination and calculate zACH values to evaluate the effectiveness of various air cleaning strategies in reducing inter-zonal transmission risk. However, steady-state analysis alone cannot account for transient conditions related to outdoor climate, occupant movement, and air cleaning system operation schedules.

Based on the steady-state simulation results, we designed transient simulations to estimate transmission risk, considering the dynamic outdoor wind environment and the movement of the index case in guest rooms, corridor, and the common room. This way, we could consider different possibilities for airborne transmission on the floor beyond just inter-zonal transmission from the index case room, which was evaluated

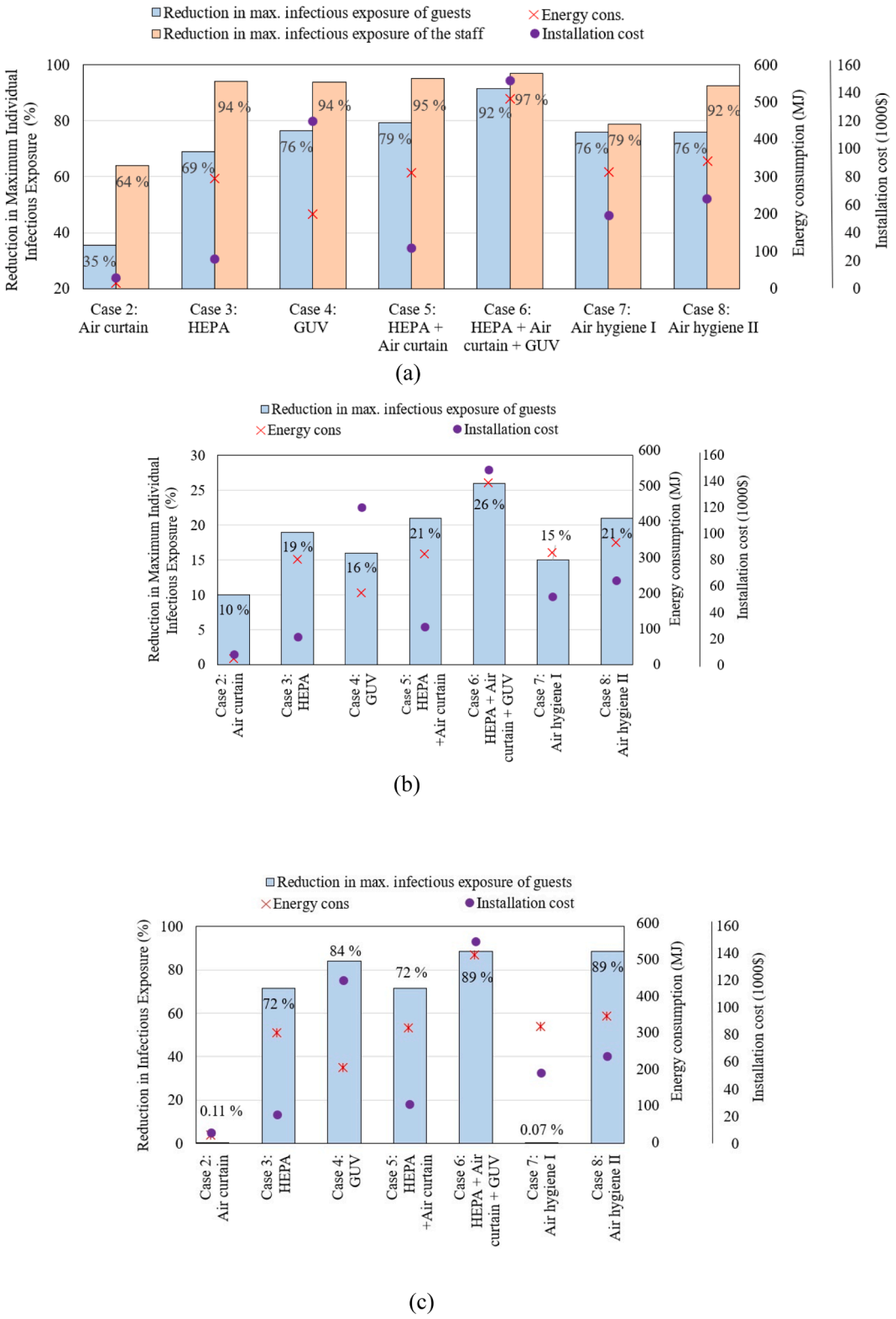

Fig. 12. Reduction in the maximum individual infectious exposure with different air cleaning strategies, along with associated installation cost and energy consumption. Bars represent exposure reduction (left axis); markers represent installation cost and energy consumption (right axes).

in the steady-state simulations. Transient simulations enabled a more realistic assessment of air cleaning strategies. Notably, this method allowed us to incorporate a schedule for door opening and closing into the simulations, which has been recognized as a factor in inert-zonal transmission in quarantine hotels [6].

4.2. *Appropriate application for air cleaning strategies*

We evaluated the performance of seven air cleaning strategies, comprising HEPA air cleaners, GUV fixtures, and filtered air curtains in reducing infectious exposure. The major findings are detailed below.

In our study, air supply diffusers were located in the corridors. With

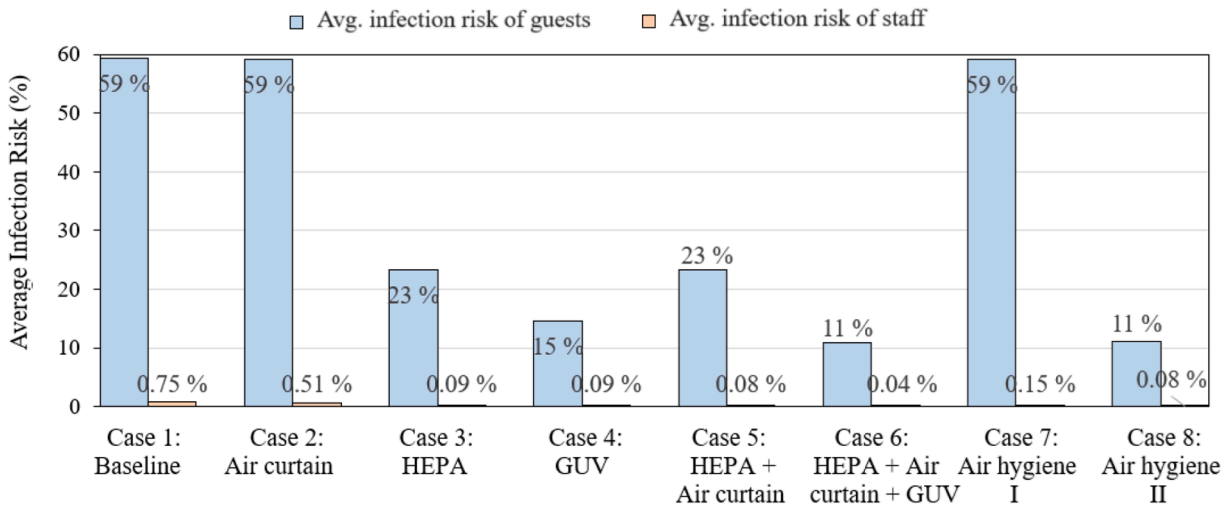

Fig. 13. Average infection risk under various air cleaning strategies.

an airtight building envelope, this ventilation design isolates quarantine rooms by directing air from the corridor into the rooms [51]. However, due to insufficient airtightness in the current study, the positive pressure in the corridor was inadequate to significantly shift the neutral plane at the doorway and establish a one-way flow from the corridor to the rooms. Consequently, air curtains played a crucial role in effectively minimizing the escape of the contaminated air from the rooms, even when the room maintained a positive pressure relative to the corridor, up to a certain threshold. This rose a concern that viral aerosols might enter the room from the corridor, potentially causing cross-transmission to healthy residents. To address this, we attached a MERV-13 filter to the air curtain's intake grill, which proved effective. However, it should be noted that adding a MERV-13 filter also reduced the supply airflow rate. Another advantage of air curtains is their low initial and operational costs, as they only operate when the door is open, typically lasting just a few minutes in quarantine facilities. Finally, it is important to note that the use of air curtains requires sufficient space above the top of the door frame, making them not always applicable.

HEPA air cleaners and GUV fixtures can significantly reduce the risk of airborne transmission through effective source control, but they also have limitations. With HEPA air cleaners, noise is a concern, as it is directly related to fan speed and the provided CADR. This makes it challenging to design an effective yet quiet air cleaning strategy using HEPA air cleaners. For GUV fixtures, their use is constrained by UV exposure guidelines [52]. Additionally, GUV fixtures can produce ozone and particulate matter (PM) in indoor environments [53], necessitating caution when designing air cleaning strategies for spaces where occupants may be exposed for extended periods, such as the common room. Additionally, GUV fixtures are relatively more expensive than HEPA air cleaners. On the other hand, they consume significantly less energy.

According to the transient simulation results, air cleaning performance does not change linearly with the level of air cleaning deployments. Therefore, both initial and operational costs, as well as energy considerations, should be taken into account when developing an effective air cleaning strategy for a specific objective. For instance, when aiming to reduce inter-zonal transmission, both air hygiene I and II strategies can effectively protect guests from inter-zonal transmission. While the air hygiene I strategy was more cost-efficient, the air hygiene II strategy provided a safer environment in the common room area.

The transient simulation results also highlighted the challenge of controlling transmission risk from dynamic sources, such as an index case walking in the corridor. In addition to implementing air cleaning strategies, mask-wearing in these public areas is highly recommended. Moreover, our simulation results indicated that even with extensive air cleaning strategies, the infection risk in a gathering space may not be reduced to an acceptable level, as evidenced by an equivalent 9.6 % infection risk in the common room when using HEPA air cleaners and GUV fixtures. Therefore, it is crucial to maintain strict distancing of occupants in public spaces during pandemics.

4.3. *Limitation of multizone model simulation*

This study used validated multi-zone modeling of an actual quarantine hotel floor. With a perfect mixing assumption, contaminant properties were considered uniform within each zone. Multi-zone modeling does not account for airflow patterns and localized air mixing in individual zones, such as rooms. By nature, multi-zone modeling cannot account for the effects of turbulent airflows, such as exhaled airflow and air jets from HEPA air cleaners, on aerosol spread [54,55]. Notably, the multi-zone model cannot capture airborne transmission occurring in close proximity to the index case. Consequently, it might overestimate the effectiveness of air cleaning systems within the same zone. Thus, within-room airborne transmission risk may be more significant, if social distancing rules are not applied. Additionally, we did not consider the effects of surrounding buildings on wind conditions, which will be analyzed in our future research by coupling the multi-zone modeling with CFD to incorporate the outdoor environment, considering the impact of the local urban landscape [56]. It is conceivable that surrounding buildings could affect the wind flow around the building, influencing the pressure distribution over its exterior envelope and, consequently, air infiltration into the building.

5. Conclusions

This study addresses the need for designing effective and practical air cleaning strategies for hotels repurposed as quarantine facilities. We assessed the effectiveness of seven air cleaning strategies, comprising HEPA air cleaners, GUV fixtures, and air curtains, both individually and in combination, to convert an ordinary hotel floor into a quarantine facility without renovating the HVAC system. The assessment used a comprehensive, validated multi-zone model to evaluate the reduction in dispersion of viral aerosols within a quarantine hotel floor. The calibration process included data collected in an actual hotel that served as a quarantine facility during the CVID-19 pandemic. We identified critical areas for airborne transmission, such as guest rooms at the corridor ends, the common room, and corridors in front of elevator shafts, highlighting the importance of deploying air cleaning devices in these locations. Strategies comprising only HEPA air cleaners and only GUV fixtures significantly reduced inter-zonal transmission risk through strong source control capabilities, achieving overall zACH values for clean air of 2.8

and 3.5 1/h, respectively. Air curtains effectively minimized the escape rate of contaminated air into the corridor. Importantly, incorporating MERV-13 filters into air curtains further reduced contaminant concentration in the rooms by 56 % when the source was located in the corridor.

Considering space constraints in an actual quarantine facility, we proposed two strategies combining different air cleaning devices, called air hygiene I (focused on air cleaning in individual rooms) and air hygiene II (addressing both individual rooms and the common room), which effectively protected occupants from inter-zonal transmission. These strategies primarily used HEPA air cleaners and air curtains due to their cost-effectiveness, supplemented by a limited number of GUV fixtures. We found that increasing the number of deployed air cleaning devices in a quarantine facility did not result in a proportional reduction in infectious exposure, highlighting the importance of balancing mitigation performance with installation costs and energy consumption considerations. Although the HEPA + air curtain + GUV strategy had initial costs 2.9 and 2.3 times higher than air hygiene I and II strategies, respectively, and energy use 1.6 and 1.5 times higher, it only provided additional reductions in the maximum individual infectious exposure of 5–18 % in the rooms compared to the exposure in the baseline model. Therefore, using a smaller number of air cleaning devices strategically place in critical floor locations is as effective as blanketing the entire hotel floor with air cleaning devices. Our findings also emphasized the necessity for over-filtering in common spaces and promoting mask-wearing in corridors.

In conclusion, our study offers an analytical framework for performance assessment of air cleaning strategies for quarantine hotels.

CRediT authorship contribution statement

Hamed Sobhani: Writing – original draft, Visualization, Validation, Software, Methodology, Investigation, Formal analysis, Data curation, Conceptualization. **Shengwei Zhu:** Writing – original draft, Investigation. **Jelena Srebric:** Writing – review & editing, Supervision, Resources, Project administration, Funding acquisition, Conceptualization.

Declaration of competing interest

All authors declare that they have no known competing financial interests or personal relationships that could have appeared to influence the work reported in this paper.

Acknowledgements

This work was funded by the National Institutes of Health, under project number 1U19AI162130 [PI: Dr. Donald K. Milton]. The authors would like to express their gratitude to Dr. Donald K. Milton (School of Public Health, University of Maryland) for providing comments and technical support and Steve Reding (Lord Baltimore Hotel) for his assistance with the installation of the equipment in the hotel.

Appendix A. Field measurements

In this section, the detailed methodology for field measurements is provided. We performed two field experiments on the quarantine hotel floor. One experiment aimed to determine the number and operation mode of HEPA air cleaners in the common room, and another was intended to collect CO_2 concentration and differential pressure data for multizone model calibration.

A.1. Determination of HEPA air cleaner deployment in the common room

As the common room was used as a physical therapy exercise area, an air change rate (ACH) of 10 1/h with 100 % outdoor air was required to meet the minimum air cleaning level suggested by the ASHRAE 62.1 Standard [49]. It was impossible to renovate the existing HVAC system to achieve such high ACH. Therefore, we decided to install multiple HEPA air cleaners (Alen, Breathsmart 45i) in the common room to achieve equivalent ACH (eACH) of 10 1/h by filtration. GUV fixtures were also added later to further increase the air cleaning level. The HEPA air cleaner had four different fan speed modes. Higher fan speeds increased air recirculation through the HEPA filter and improved filtration performance. However, they could also generate more noise, which could be acoustically uncomfortable for occupants.

To balance noise issues and filtering performance, we considered three scenarios for the use of HEPA air cleaners in the common room, including (1) three units operating at the highest (4th) fan speed, (2) four units operating at the 3rd fan speed, and (3) five units operating at the 2nd fan speed. In each scenario, the units were uniformly distributed along the walls, as shown in Fig. A.1. Noise levels were measured using a General Tools DSM402SD sound level meter. Based on the guidelines in [57], we measured the noise levels at a height of 1.2 m at eight different locations, each for 15 s. We then calculated the average noise level at each location, and then the average value in the room for each scenario. We also measured noise levels while running a single HEPA air cleaner at different fan speeds. The measurements were taken at a distance of one meter from the unit.

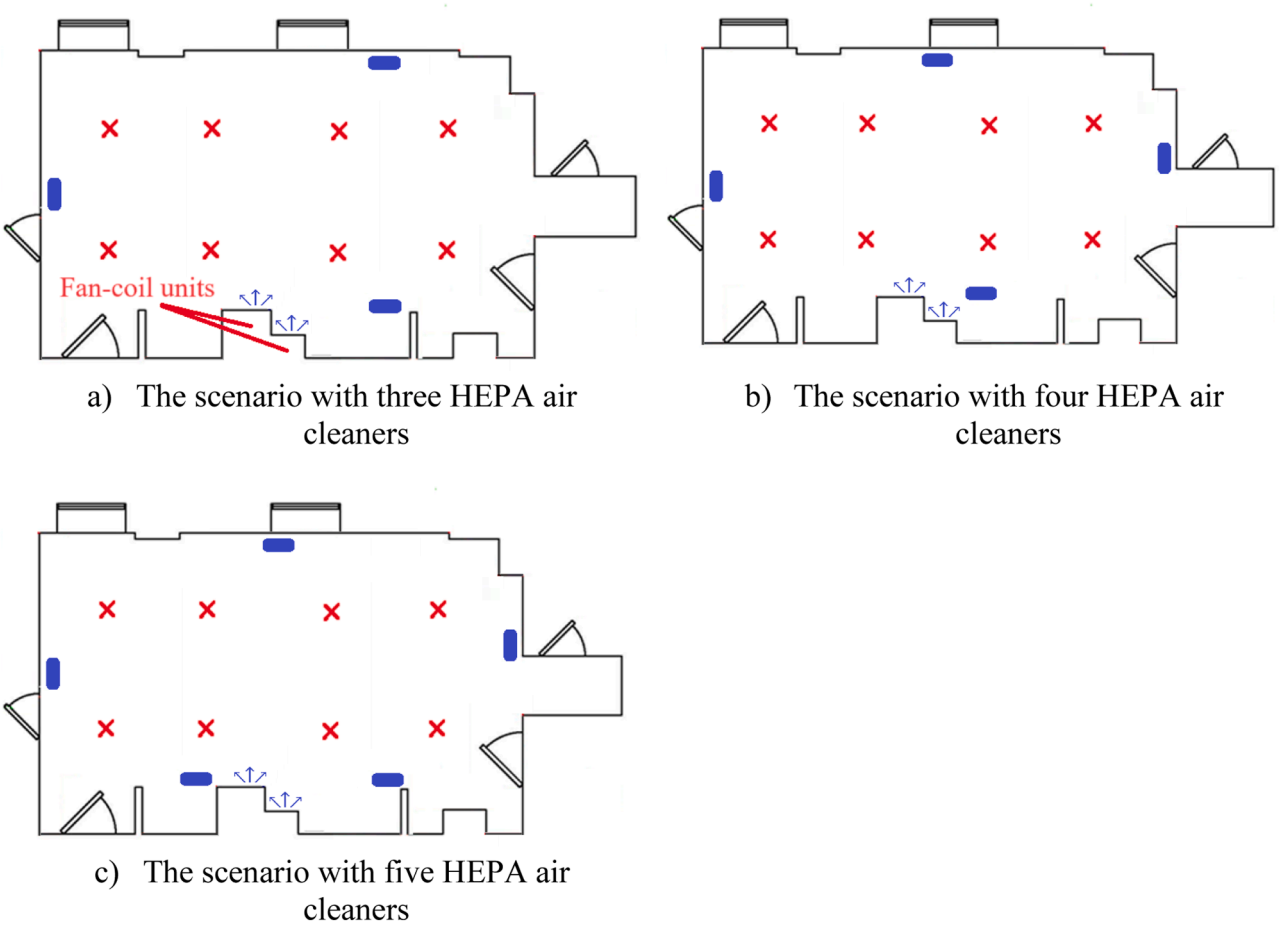

Fig. A.1. Layouts of HEPA air cleaner deployment scenarios in the common room. The small blue boxes represent the locations of HEPA air cleaners, while the crosses mark the sites selected for noise measurement.

Additionally, we measured air speed at 30 evenly distributed points on the suction opening of a HEPA air cleaner. Each measurement was taken for 10 s using a Kanomax Anemometer 6501-0E. We then calculated the airflow rate delivered at each fan speed. Given the linear relationship between clean air delivery rate (CADR) and airflow rate [58], we calculated the CADR value corresponding to each lower fan speed using the stated CADR value at the maximum fan speed (416 m^3/h [37]). The total CADR related to each scenario was then calculated as the product of the CADR value at the relevant fan speed and the number of units [59].

A.2. Data collection for multi-zone model calibration

We calibrated the multi-zone model with two types of data, including ventilation rates measured in the common room and room 1405, and the pressure difference between room 1431 and the corridor. Other than the filtration in the built-in fan-coils, no additional air cleaning systems were used during these experiments. This air cleaning setup corresponds to the baseline (case 1) model outlined in Section 2.4.

The ventilation rate in the common room and room 1405 was measured using the steady state method [60]. We released CO_2 gas into the room at a constant rate of 0.4 L/min, which was controlled by a mass flow controller (GFC171S, Aalborg Instruments & Controls Inc.). CO_2 concentrations were collected by six and four calibrated Aranet CO_2 sensors in the common room and room 1405, respectively. To evaluate the influence of air transport from adjacent areas, additional CO_2 sensors were installed in the corridor near the room doors and outdoors. To enhance the mixing of CO2 in indoor air, two HEPA air cleaners were placed in the common room and one in room 1405, all operating at maximum speed with the filters removed. Our analysis confirmed that the installed ventilation system effectively enhanced air mixing. We calculated the ventilation rates at 10 time points, spaced approximately 1 day apart for room 1405 and 3 h apart for the common room. We ensured that CO_2 concentrations in the rooms had reached steady-state conditions at the selected time points. More details about the experiments can be found in [53].

An axial window fan (Air King, 9166F) was installed in the window frame of room 1431 to form a positive pressure compared to the corridor. With three different fan speeds, we measured the pressure difference between the room 1431 and the corridor using a differential pressure sensor (HOBO, T-VER-PX3UL). During the measurements, the room door was closed.

Appendix B. Modeling of air cleaning systems

In this appendix, the methods used for modeling air cleaning systems are provided. Three air cleaning systems were considered for mitigating airborne transmission on the quarantine floor, including HEPA air cleaners, GUV fixtures, and air curtains (Fig. B.1). Each system employs a specific mechanism to reduce aerosol transmission risk. HEPA air cleaner physically captures aerosols containing viruses; GUV light inactivates viruses by disrupting their DNA or RNA [38], and the air curtain creates an air barrier at the doorway, limiting the movement of virus-laden aerosols from the

rooms to the corridor when opening the doors. This section elucidates the modeling of these systems in the multi-zone model.

a) HEPA air cleaner [37]

b) GUV fixture [47]

c) Air curtain [46]

Fig. B.1. Photos of air cleaning systems.

• HEPA air cleaners

A HEPA air cleaner was modeled as a sink with a removal rate equivalent to its CADR. The CADR values were determined based on the fan speed, as given in Table 2. HEPA air cleaners were assumed to operate at the 2nd fan speed in guest rooms and the common room to ensure an acoustically comfortable environment, while operating at the 4th fan speed in other rooms and corridors.

• GUV fixtures

GUV's removal of viral aerosols was represented as a deposition rate, calculated using the formula $k_{UV} = KI$ [61]. Here, K is the UV susceptibility constant (cm^2/mJ), and I represents the average UV fluence rate (mW/cm^2) within the zone.

To obtain I for each zone under GUV disinfection, we calculated the distributions of UV fluence rate by 222-nm far-UVC fixtures (Guard/shield, Krypton) in both the common room and a typical corridor segment. This was done using Visual Lighting, a computer-aided design (CAD) tool [62]. As the output, the software provided the volume average for I. The susceptibility constant of the virus was assumed to be 3 cm2/mJ, which is a general value for viruses such as coronavirus and influenza [63].

Upper-room GUV, which utilizes conventional 254-nm UV light, was considered unsuitable for the hotel due to the low ceiling height and long exposure periods, particularly in the rooms [33]. Alternatively, 222-nm far-UVC light is better tolerated by eyes and skin [64], allowing it to be used in occupied zones. Notably, using four GUV fixtures in the common room resulted in an average fluence rate of 0.0028 mW/cm2 on a horizontal plane 1.75 m above the floor, as a representation of the eye level. This rate did not exceed the ACGIH 8-hour exposure limit for skin (479 mJ/cm2) and eyes (161 mJ/cm2), ensuring a safe environment for occupants [53].

• Air curtains

For the air curtain, we used data corresponding to the Awoco FM3509-M model. The air curtain recirculates air by drawing corridor air from its intake grille at the top and expelling it as a downward jet from its bottom discharge nozzle. Upon reaching the floor, part of the downward airflow is deflected into the room. As a result, a net airflow from the corridor to the room occurs even if the room pressure is higher than the corridor pressure, as long as the pressure differential stays below a certain threshold. In the scenarios involving air curtains, it was assumed that they activated whenever the doors were open. The following infiltration model was applied to represent airflow through a door equipped with an air curtain [65]:

$$\frac{Q_{AC}}{A\sqrt{2/\rho}} = (-1)^i C_D \sqrt{|\Delta P_{rc}|} + D_D \tag{B.1}$$

where, Q_{AC} is the airflow rate through the door with the air curtain (m^3/s), A represents the door area (m^2), ρ is the air density (kg/m^3), and ΔP_{rc} denotes the pressure difference between the room and the corridor (Pa). C_D and D_D refer to the discharge coefficient (-) and the discharge modifier (-), respectively. The superscript i is defined based on the sign of the ΔP_{rc}: $i = 0$ when $\Delta P_{rc} \geq 0$, and $i = 1$ when $\Delta P_{rc} < 0$.

We fitted this model to the airflow-pressure difference curves reported in [66] for air curtains operating at supply air velocities of 10 m/s and 16

m/s . This way, we could find the values for CD and DD. These velocities corresponded to average values obtained from our measurements at 64 points across the outlet of the air curtain, with and without a MERV-13 filter, respectively. We then developed airflow-pressure difference curves specific to the hotel room doors, as shown in Fig. B.2. We imported the data into CONTAM using the "Q vs P" fit model.

Note that the airflow-pressure difference curves exhibit sharp angles at two points: the upper critical pressure difference (ΔPuc) and the lower critical pressure difference (ΔPlc). We have shown these points for the standard air curtain in Fig. B.2. The position of ΔPrc relative to these critical points determines how the pressure difference interacts with the air curtain to influence airflow pattern through the door. For more detailed information, please refer to [65]. Accordingly, we derived separate CD and DD coefficients for the three segments of the curves: $\Delta Prc \geq \Delta Puc$, $\Delta Prc \leq \Delta Plc$, and $\Delta Plc < \Delta Prc < \Delta Puc$. For the filtered air curtain, a filter element was also incorporated into the model.

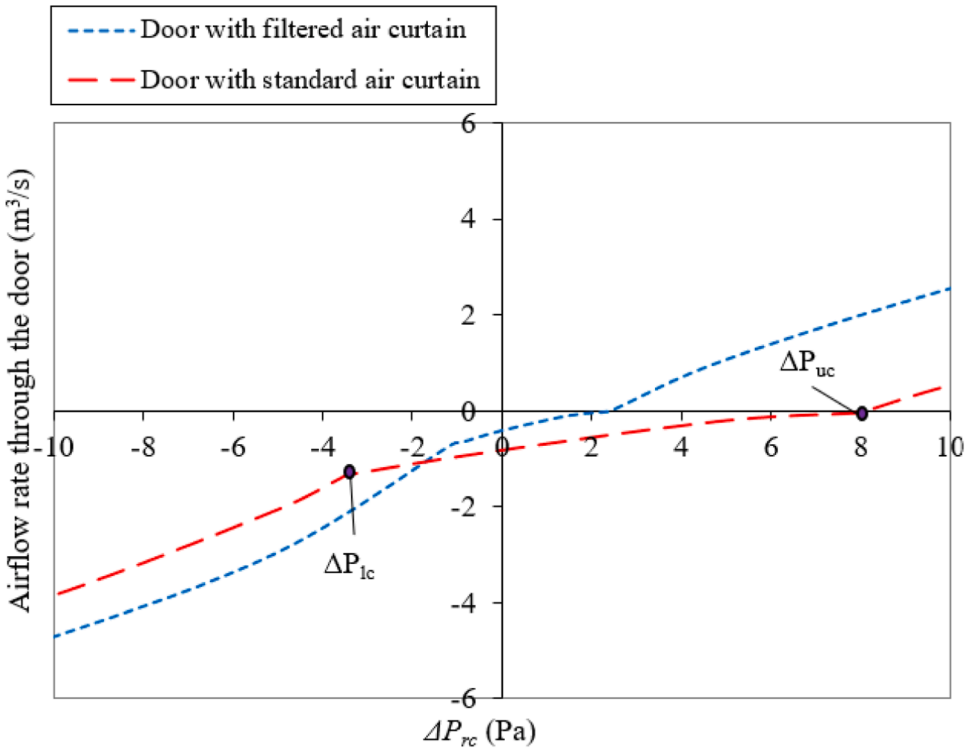

Fig. B.2. Developed infiltration models for a door equipped with an air curtain, with and without MERV-13 filter using data from [66]. A positive airflow rate indicates airflow from the room to the corridor. The standard air curtain refers to an air curtain without a filter.

Appendix C. Air cleaning system configurations for different strategies

The configuration of air cleaning systems for different modeled strategies is shown in Fig. C.1.

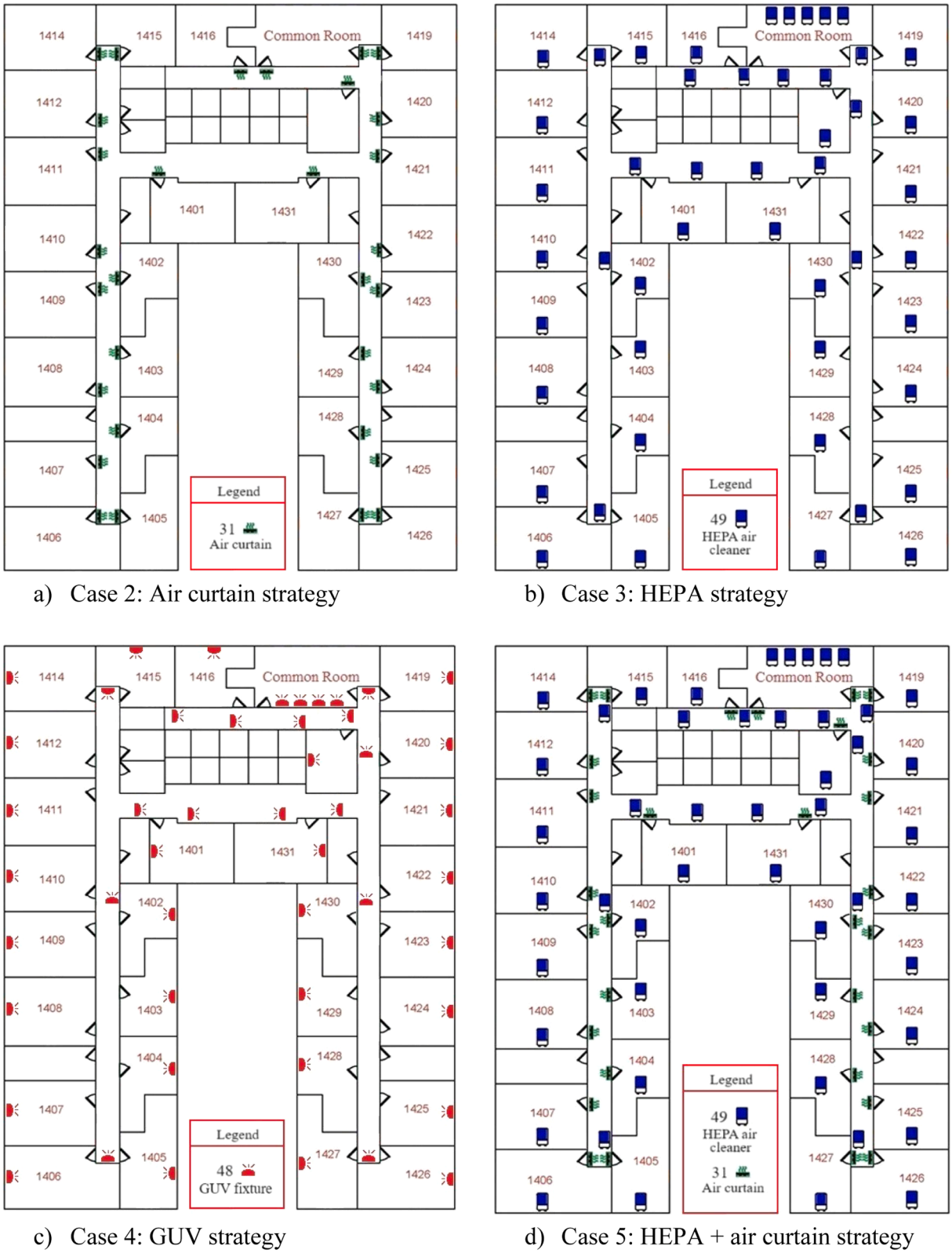

a) Case 2: Air curtain strategy

b) Case 3: HEPA strategy

c) Case 4: GUV strategy

d) Case 5: HEPA + air curtain strategy

Fig. C.1. Schematic layout of air cleaning system deployment for different strategies.

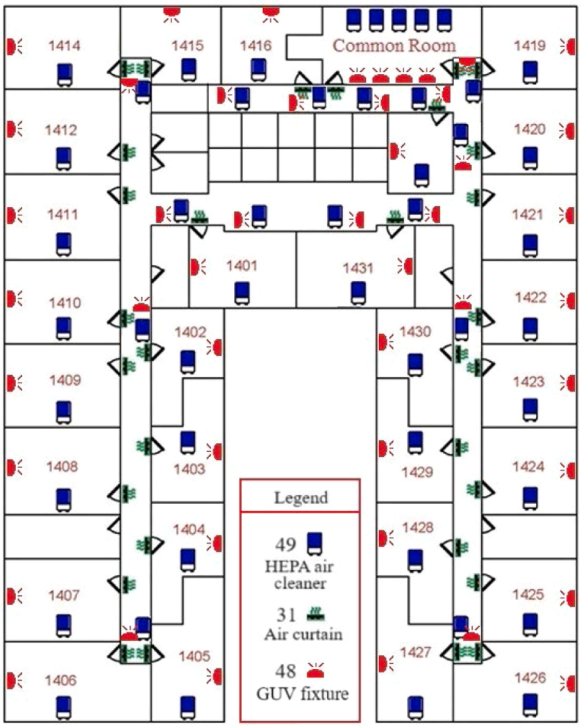

e) Case 6: HEPA+ air curtain + GUV strategy

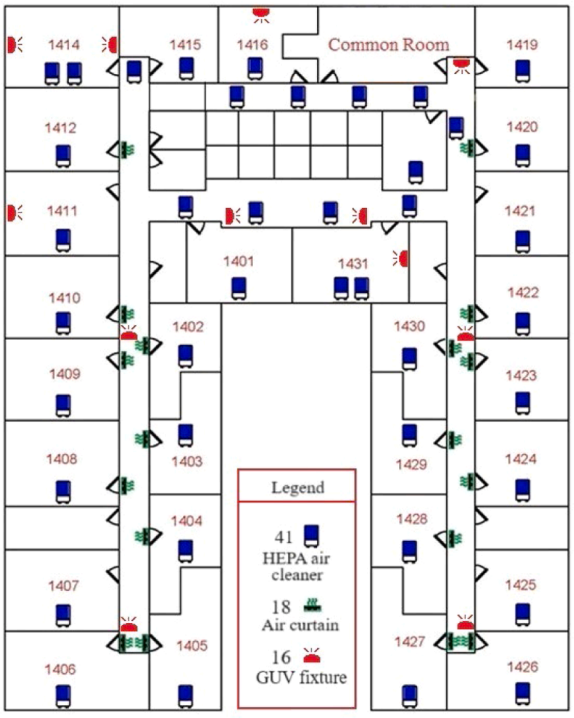

f) Case 7: Air hygiene I strategy

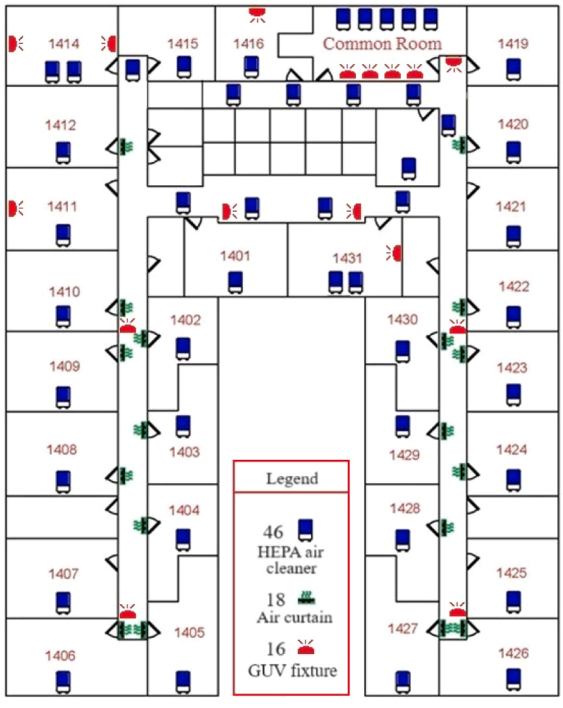

g) Case 8: Air hygiene II strategy

Fig. C.1. (*continued*).

Appendix D. Procedure for zACH Calculation

This section details the calculation procedure for the inter-zonal air exchange rate (zACH) index.

Step 1: For a selected air cleaning strategy, place the index case in one potential location and calculate the steady-state quanta concentrations across all zones with all doors open. As an example, we consider the HEPA strategy (Fig. C.1(b)) and position the index case in Room 1402. Table D.1

shows the steady-state quanta concentrations in a few spaces.

Table D.1
Steady-state quanta concentrations across zones with the source in room 1402 (before adjustments).

	Steady-state quanta conc. (quanta/m3)										
Source location	Room 1401	Room 1402	Room 1403	Room 1404	Room 1405	Room 1406	Room 1407	Room 1408	Room 1409	…	Electrical room
Room 1402	0	0.11	0.0049	0.0035	0.00071	0.00069	0.0018	0.0048	0.0078	…	0

Step 2: Set the quanta concentration at the source location to zero to focus exclusively on inter-zonal transmission to other spaces. The adjusted concentrations are presented in Table D.2.

Table D.2
Steady-state quanta concentrations across zones with the source in room 1402 (after adjustments).

	Steady-state quanta conc. (quanta/m3)										
Source location	Room 1401	Room 1402	Room 1403	Room 1404	Room 1405	Room 1406	Room 1407	Room 1408	Room 1409	…	Electrical room
Room 1402	0	0	0.0049	0.0035	0.00071	0.00069	0.0018	0.0048	0.0078	…	0

Step 3: Repeat the procedure for other potential source locations. For each case, calculate the steady-state quanta concentrations and then set the source location's concentration to zero. Table D.3 summarizes the results for various source locations.

Table D.3
Steady-state quanta concentrations for all source locations.

	Steady-state quanta conc. (quanta/m3)									
Source location	Room 1401	Room 1402	Room 1403	Room 1404	Room 1405	Room 1406	Room 1407	Room 1408	…	Electrical room
Room 1402	0	0	0.0049	0.0035	0.00071	0.00069	0.0018	0.0048	…	0
Room 1403	0	0	0	0.010	0.0020	0.0020	0.0053	0.014		0
Room 1404	0	0	0.000024	0	0.0049	0.0048	0.0128	0.000084		0
Room 1405	0	0	0	0	0	0.013	0	0		0
Room 1406	0	0	0	0	0.013	0	0	0		0
Room 1408	0	0	0.015	0.011	0.0022	0.0021	0.0056	0		0
Room 1409	0	0	0.010	0.0074	0.0015	0.0015	0.0039	0.010		0
Room 1410	0	0.010	0.0047	0.0033	0.00068	0.00066	0.0018	0.0045		0
Room 1412	0	0	0	0	0	0	0	0		0
Common room	0	0	0	0	0	0	0	0		0
Room 1420	0	0	0	0	0	0	0	0		0
Room 1422	0	0	0	0	0	0	0	0		0
Room 1423	0	0	0	0	0	0	0	0		0
Room 1424	0	0	0	0	0	0	0	0		0
Room 1426	0	0	0	0	0	0	0	0		0
Room 1427	0	0	0	0	0	0	0	0		0
Room 1428	0	0	0	0	0	0	0	0		0
Room 1429	0	0	0	0	0	0	0	0		0
Room 1430	0	0	0	0	0	0	0	0		0

Step 4: Calculate the average quanta concentration for each zone using the results from Step 3. The average values are shown in Table D.4.

Table D.4
Average quanta concentrations for the zones.

Average quanta conc. (quanta/m3)										
Room 1401	Room 1402	Room 1403	Room 1404	Room 1405	Room 1406	Room 1407	Room 1408	Room 1409	…	Electrical room
0	0.00056	0.0019	0.0019	0.0014	0.0014	0.0016	0.0018	0.00084	…	0

Step 5: Determine the volume-weighted average quanta concentration for the entire floor (C_{ss}, quanta/m^3) for the selected air cleaning strategy using:

$$C_{ss} = \frac{1}{V}\sum (C_i.\ V_i) \tag{D.1}$$

where, C_i is the average quanta concentration in zone i, V_i is the volume of zone i, and V is the total floor volume.

Step 6: As we set the quanta concentration in the source locations, the source quanta generation rate cannot be directly used to calculate zACH. Instead, the equivalent quanta is determined based on the quanta concentrations in zones other than the source location. This involves calculating the volume-weighted average quanta concentration throughout across the entire floor for the scenario without air cleaning systems and fan-coil filtration

($C_{ss,b}$, quanta/m^3), following the methodology described in Steps 1–5. The equivalent quanta generation rate is then computed using the following equation:

$$G_e = QC_{ss,b} \tag{D.2}$$

where, Q is the rate of clean airflow entering the floor.

Step 7: Finally, calculate the zACH using the following equation:

$$zACH = \frac{G_e}{C_{ss}V} - \frac{Q}{V} \tag{D.3}$$

Data availability

The data that has been used is confidential.

References

[1] National Review of Hotel Quarantine, Australian Government Department of Health and Aged Care, 2020.

[2] S.A. Rella, Y.A. Kulikova, E.T. Dermitzakis, F.A. Kondrashov, Rates of SARS-CoV-2 transmission and vaccination impact the fate of vaccine-resistant strains, Sci. Rep. 11 (2021) 15729.

[3] World Health Organization. Scientific Brief: Transmission of SARS-CoV-2: Implications for Infection Prevention Precautions [Internet]. World Health Organization (WHO); 2020 Jul 9 [cited 2024 Aug 6]; Available from: https://www.who.int/news-room/commentaries/detail/transmission-of-sars-cov-2-implications-for-infection-prevention-precautions.

[4] CDC, Science Brief: SARS-CoV-2 and Potential Airborne Transmission [Internet], Centers for Disease Control and Prevention, 2020 [cited 2021 Mar 17]; Available from, https://www.cdc.gov/coronavirus/2019-ncov/more/scientific-brief-sars-cov-2.html.

[5] K.W. Chia, J. Xiong, Once upon a time in quarantine: exploring the memorable quarantine hotel experiences of Chinese student returnees during the COVID-19 pandemic, Tour. Hospit. Res. 23 (2023) 72–87.

[6] S. Wong, H. Chen, D.C. Lung, P. Ho, K. Yuen, V.C. Cheng, To prevent SARS-CoV-2 transmission in designated quarantine hotel for travelers: is the ventilation system a concern? Indoor Air 31 (2021) 1295–1297.

[7] Australian Health Protection Principal Committee (AHPPC) Statement on Australia's National Hotel Quarantine Principles, 2020.

[8] L. Grout, A. Katar, D. Ait Ouakrim, J.A. Summers, A. Kvalsvig, M.G. Baker, et al., Failures of quarantine systems for preventing COVID-19 outbreaks in Australia and New Zealand, Medical J. Austral. 215 (2021) 320–324.

[9] B. Haire, G.L. Gilbert, J.M. Kaldor, D. Hendrickx, A. Dawson, J.H. Williams, Experiences of risk in Australian hotel quarantine: a qualitative study, BMC Public Health 22 (2022) 953.

[10] D. Dincer, O. Gocer, Quarantine hotels: the adaptation of hotels for quarantine use in Australia, Buildings 11 (2021) 617.

[11] S. Zhu, S. Jenkins, K. Addo, M. Heidarinejad, S.A. Romo, A. Layne, et al., Ventilation and laboratory confirmed acute respiratory infection (ARI) rates in college residence halls in College Park, Maryland, Environ. Int. 137 (2020) 105537.

[12] CDC, About Ventilation and Respiratory Viruses [Internet], Ventilation, 2024 [cited 2024 Dec 12];Available from, https://www.cdc.gov/niosh/ventilation/about/index.html.

[13] F.T. Lu, R.J. Laumbach, A. Legard, N.T. Myers, K.G. Black, P. Ohman-Strickland, et al., Real-world effectiveness of portable air cleaners in reducing home particulate matter concentrations, Aerosol. Air. Qual. Res. 24 (2024) 230202.

[14] M. Sheraz, H.N. Ly, V.C. Thi Le, V.Q. Nguyen, F.H. Naqvi, J.Y. Park, et al., Electrospinning synthesis of CuBTC/TiO2/PS composite nanofiber on HEPA filter with self-cleaning property for indoor air purification, Process Saf. Environ. Protect. 172 (2023) 621–631.

[15] E.R. Blatchley, D.J. Brenner, H. Claus, T.E. Cowan, K.G. Linden, Y. Liu, et al., Far UV-C radiation: an emerging tool for pandemic control, Crit. Rev. Environ. Sci. Technol. 53 (2023) 733–753.

[16] M. Buonanno, N.J. Kleiman, D. Welch, R. Hashmi, I. Shuryak, D.J. Brenner, 222 nm far-UVC light markedly reduces the level of infectious airborne virus in an occupied room, Sci. Rep. 14 (2024) 6722.

[17] P. Li, J.A. Koziel, R.V. Paris, N. Macedo, J.J. Zimmerman, D. Wrzesinski, et al., Indoor air quality improvement with filtration and UV-C on mitigation of particulate matter and airborne bacteria: monitoring and modeling, J. Environ. Manage 351 (2024) 119764.

[18] W. Dols, B. Polidoro, CONTAM User Guide and Program Documentation Version 3.4, National Institute of Standards and Technology (NIST, 2021.

[19] P. Shrestha, J.W. DeGraw, M. Zhang, X. Liu, Multizonal modeling of SARS-CoV-2 aerosol dispersion in a virtual office building, Build. Environ. 206 (2021) 108347.

[20] G. Guyot, S. Sayah, S. Guernouti, A. Mélois, Role of ventilation on the transmission of viruses in buildings, from a single zone to a multizone approach, Indoor Air 32 (2022) e13097.

[21] S. Yan, L (Leon) Wang, M.J. Birnkrant, Z (John) Zhai, S.L Miller, Multizone modeling of airborne SARS-CoV-2 quanta transmission and infection mitigation strategies in office, hotel, retail, and school buildings, Buildings 13 (2023) 102.

[22] Evaluating Modes of Influenza Transmission (EMIT-2) Using Innovative Technologies and Designs in Controlled Environments [Internet]. NIH Report 2021 [cited 2024 Jul 31]; Available from: https://reporter.nih.gov/search/cK_8orEFTkiFt2Lg8byE6w/project-details/10260845.

[23] Climomaster Anemometer –6501 Series, Climomaster probe Specifications [Internet], 2024. Available from, https://kanomax-usa.com/products/climomaster-anemometer-6501-series/.

[24] NIST, Miscellaneous Residential Leakage Data [Internet], National Institute of Standard and Technology, 2018 [cited 2024 Jun 1]; Available from: https://www.nist.gov/el/energy-and-environment-division-73200/nist-multizone-modeling/software/contam/input-data.

[25] C. Reinhold, R. Sonderegger, Component Leakage Areas in Residential Buildings [Internet], 1983 [cited 2024 Jul 12]. Available from, https://www.semanticscholar.org/paper/Component-leakage-areas-in-residential-buildings-Reinhold-Sonderegger/6d8176a0e6f1a6bfc052d6a360c4e8edd1ec9c2e.

[26] R.S. Miller, D. Beasley, On stairwell and elevator shaft pressurization for smoke control in tall buildings, Build. Environ. 44 (2009) 1306–1317.

[27] NIST,ASHRAE Table of Residential Leakage Data [Internet], National Institute of Standard and Technology, 2018 [cited 2024 Jun 1]; Available from: https://www.nist.gov/el/energy-and-environment-division-73200/nist-multizone-modeling/software/contam/input-data.

[28] NIST, Miscellaneous Commercial and Institutional Building Airtightness Data [Internet], National Institute of Standard and Technology, 2018. [cited 2024 Jun 1]; Available from: https://www.nist.gov/el/energy-and-environment-division-73200/nist-multizone-modeling/software/contam/input-data.

[29] W.F. Wells, M.W. Wells, T.S. Wilder, The environmental control of epidemic contagion: an epidemiologic study of radiant disinfection of air in day schools, Am. J. Epidemiol. 35 (1942) 97–121.

[30] G. Buonanno, L. Stabile, L. Morawska, Estimation of airborne viral emission: quanta emission rate of SARS-CoV-2 for infection risk assessment, Environ. Int. 141 (2020) 105794.

[31] P. Fabian, J.J. McDevitt, W.H. DeHaan, R.O.P. Fung, B.J. Cowling, K.H. Chan, et al., Influenza virus in human exhaled breath: an observational study, PLoS ONE 3 (2008) e2691.

[32] T. Hussein, J. Löndahl, S. Thuresson, M. Alsved, A. Al-Hunaiti, K. Saksela, et al., Indoor Model Simulation for COVID-19 Transport and Exposure, Int. J. Environ. Res. Public Health 18 (2021) 2927.

[33] S. Zhu, T. Lin, L. Wang, E.A. Nardell, R.L. Vincent, J. Srebric, Ceiling impact on air disinfection performance of Upper-Room Germicidal Ultraviolet (UR-GUV), Build. Environ. 224 (2022) 109530.

[34] P.J. Bueno de Mesquita, C.J. Noakes, D.K. Milton, Quantitative aerobiologic analysis of an influenza human challenge-transmission trial, Indoor Air 30 (2020) 1189–1198.

[35] W.S. Dols, B.J. Polidoro, D. Poppendieck, S.J. Emmerich, A Tool to Model the Fate and Transport of Indoor Microbiological Aerosols (FaTIMA), U.S. Department of Commerce, National Institute of Standards and Technology (NIST, 2020.

[36] Doremalen N van, Bushmaker T, D.H. Morris, M.G. Holbrook, A. Gamble, B. N. Williamson, et al., Aerosol and surface stability of SARS-CoV-2 as compared with SARS-CoV-1, N. Engl. J. Med. 382 (2020) 1564–1567.

[37] Alen BreatheSmart 45i HEPA Air Purifier [Internet], 2024. Available from, https://alen.com/products/breathesmart-45i.

[38] H. Sobhani, H. Shokouhmand, Effects of number of low-pressure ultraviolet lamps on disinfection performance of a water reactor, J. Water. Process. Eng. 20 (2017) 97–105.

[39] D. Koenigshofer, J. Murphy, W. Grondzik, HVAC Design Manual For Hospitals and Clinics, 2nd ed, ASHRAE, 2013.

[40] S.N. Rudnick, J.J. McDevitt, G.M. Hunt, M.T. Stawnychy, R.L. Vincent, P. W. Brickner, Influence of ceiling fan's speed and direction on efficacy of upperroom, ultraviolet germicidal irradiation: experimental, Build. Environ. 92 (2015) 756–763.

[41] Glen Burnie, MD Weather History [Internet]. [cited 2024 Feb 10]; Available from: https://www.wunderground.com/history/daily/us/md/baltimore/KBWI.

[42] F. Borghi, A. Spinazzè, S. Mandaglio, G. Fanti, D. Campagnolo, S. Rovelli, et al., Estimation of the inhaled dose of pollutants in different micro-environments: a systematic review of the literature, Toxics 9 (2021) 140.

[43] A. Sohani, M.H. Shahverdian, H. Sayyaadi, S. Nižetić, M.H. Doranehgard, An optimum energy, economic, and environmental design based on DEVAP concept to reach maximum heat recovery in a PV-wind turbine system with hydrogen storage, Energy Convers. Manage. 288 (2023) 117147.
[44] A. Sohani, C. Cornaro, M.H. Shahverdian, D. Moser, M. Pierro, A.G. Olabi, et al., Techno-economic evaluation of a hybrid photovoltaic system with hot/cold water storage for poly-generation in a residential building, Appl. Energy 331 (2023) 120391.
[45] H. Sobhani, F. Shahmoradi, B. Sajadi, Optimization of the renewable energy system for nearly zero energy buildings: a future-oriented approach, Energy Convers. Manage 224 (2020) 113370.
[46] Awoco, FM35-M Elegant 2 Speeds Air Curtain, UL Certified, 120V Unheated With an Easy-Install Magnetic Switch [Internet], 2024. Available from, https://awoco.com/collections/elegant/products/awoco-fm35-m-elegant-2-speeds-air-curtain-ul-certified-with-an-easy-install-magnetic-switch.
[47] Far UV Technologies, Krypton-Guard/Shield [Internet], 2024. Available from, https://faruv.com/disinfection-floor-lamp/.
[48] Jareemit D., Shu S., Srebric J. A Field Investigation of Air Infiltration Rates Through Automatic Entrance Doors in Retail Buildings.
[49] ANSI/ASHRAE Standard 62.1-2022: Ventilation and Acceptable Indoor Air Quality, 2022.
[50] A. Iten, T. Bouvard, Y. Thomas, C. Bonfillon, C. Ginet, L. Kaiser, et al., P038: efficacy of prevention measures against nosocomial influenza at a large university hospital, Antimicrob. Resist. Infect. Control 2 (2013) P38.
[51] P. Cheng, W. Chen, S. Xiao, F. Xue, Q. Wang, P.W. Chan, et al., Probable cross-corridor transmission of SARS-CoV-2 due to cross airflows and its control, Build. Environ. 218 (2022) 109137.
[52] Threshold limit values and biological exposure indices, in: American Conference of Governmental Industrial Hygienists (ACGIH), 2020.
[53] P. Kalliomäki, H. Sobhani, P. Stratton, K.K. Coleman, A. Srikakulapu, R. Salawitch, et al., Ozone and Ultra-Fine Particle Concentrations in a Hotel Quarantine Facility During 222 Nm far-UVC Air Disinfection [Internet], 2023 [cited 2024 Aug 1]; Available from, http://medrxiv.org/lookup/doi/10.1101/2023.09.29.23296366.
[54] S. Yan, L (Leon) Wang, M.J. Birnkrant, J. Zhai, S.L Miller, Evaluating SARS-CoV-2 airborne quanta transmission and exposure risk in a mechanically ventilated multizone office building, Build. Environ. 219 (2022) 109184.
[55] C.J. Noakes, M.A.I. Khan, C.A. Gilkeson, Modeling infection risk and energy use of upper-room Ultraviolet Germicidal Irradiation systems in multi-room environments, Sci. Technol. Built. Environ. 21 (2015) 99–111.
[56] L.L. Wang, W.S. Dols, Q. Chen, Using CFD capabilities of CONTAM 3.0 for simulating airflow and contaminant transport in and around buildings, HVAC&R. Res. 16 (2010) 749–763.
[57] ASHRAE Handbook—HVAC Applications. Chapter 48, Noise and Vibration Control, 2011.
[58] J.H. Sung, Y. Lee, B. Han, Y.J. Kim, H.J. Kim, Improvement of particle clean air delivery rate of an ion spray electrostatic air cleaner with zero-ozone based on diffusion charging, Build. Environ. 186 (2020) 107335.
[59] K.C. Noh, S.J. Yook, Evaluation of clean air delivery rates and operating cost effectiveness for room air cleaner and ventilation system in a small lecture room, Energy Build. 119 (2016) 111–118.
[60] S. Batterman, Review and extension of CO2-based methods to determine ventilation rates with application to school classrooms, Int. J. Environ. Res. Public Health 14 (2017) 145.
[61] S. Park, R. Mistrick, D. Rim, Performance of upper-room ultraviolet germicidal irradiation (UVGI) system in learning environments: effects of ventilation rate, UV fluence rate, and UV radiating volume, Sustain. Cities. Soc. 85 (2022) 104048.
[62] S.N. Rudnick, M.W. First, T. Sears, R.L. Vincent, P.W. Brickner, P.Y. Ngai, et al., Spatial distribution of fluence rate from upper-room ultraviolet germicidal irradiation: experimental validation of a computer-aided design tool, HVAC&R. Res. 18 (2012) 774–794.
[63] H. Sobhani, S. Zhu, R.L. Vincent, H.D. Costa, Srebric J. A literature review of ultraviolet inactivation rate constants (k-values) for the most frequently studied microorganisms (1854-RP), Sci. Technol. Built Environ (2025) under review.
[64] E. Eadie, I.M.R. Barnard, S.H. Ibbotson, K. Wood, Extreme exposure to filtered far-UVC: a case study†, Photochem. Photobiol. 97 (2021) 527–531.
[65] L (Leon) Wang, Z. Zhong, An approach to determine infiltration characteristics of building entrance equipped with air curtains, Energy Build. 75 (2014) 312–320.
[66] C. Shu, L (Leon) Wang, C. Zhang, D. Qi, Air curtain effectiveness rating based on aerodynamics, Build. Environ. 169 (2020) 106582.